Electronic Supplementary Information

Synthesis, photophysical characterisation, quantum-chemical study and *in vitro* antiproliferative activity of cyclometalated Ir(III) complexes based on 3,5-dimethyl-1-phenyl-*1H*-pyrazole and N,N-donor ligands

Materials and physical measurements

Analytical grade solvents and commercially available compounds were used as received. Elemental analysis was run on an Elementar Vario Micro Cube analyzer (Elementar, Germany). The FTIR spectra were recorded on a Nicolet 380 spectrophotometer (Thermo Fisher Scientific, USA) in the spectral range 4000–400 cm^{-1} using the KBr discs method. UV-Vis measurements in acetonitrile or dichloromethane solutions were performed on a UV-Vis spectrophotometer (V-630 JASCO, Japan) using 1 cm cuvettes. All absorbance measurements were recorded at room temperature and concentrations $1 \cdot 10^{-4}$–10^{-6} M for ligands and complexes (**1–4**). A micrOTOF-Q II (Brucker) was used to record the ESI-MS spectra of the complexes CH_3CN or MeOH solutions. The thermal stability of the selected complexes was carried out using a Q50 thermobalance manufactured by TA Instruments Inc. coupled with a Nicolet iS10 FT-IR spectrometer under a nitrogen flow from 25 °C to 1000 °C at a heating rate of 4 °C·min^{-1}. The corrected steady-state luminescence spectra were recorded with Gilden Photonics FluoroSense fluorimeter. The measurements at 298 K were performed in 1×1 cm fused silica cells fulfilled with the investigated complex solutions thoroughly deaerated by the prolonged saturation with preliminary purified and dried argon. The emission quantum yields ϕ_{em} (with an estimated error of *ca.* ±10%) were determined in relation to a solution of quinine sulphate in 0.1 N H_2SO_4 in aerated acetonitrile solutions served as a reference luminophore with ϕ_{em} = 0.51.[1] The 77 K measurements were performed in NMR like fused silica tubes with 3 mm inner diameter by placing them in a liquid nitrogen filled Dewar flask with a bottom transparent finger. The emission decays were recorded with FluoroSense-P fluorimeter especially designed to the time-resolved measurements in the microsecond range with the temporal resolution of 0.01 μs. In the performed lifetime measurements. The experimental decay curves were analyzed by the single-curve method using the reference convolution based on the Marquardt algorithm[2] with the χ^2 values (close to unity), the distributions of residuals, and the adjusted coefficients of determination R^2 values (at least 0.995) served as the criteria in the evaluation of the fit quality. The lifetime τ_{em} values were determined with an estimated error of *ca.* ±10%. Circular dichroism spectra were recorded with a Jasco J-815 spectropolarimeter (Jasco Inc., Austria). The NMR spectra were recorded either on Varian VNMRS-500 (Varian Inc., USA) or Varian VNMRS-600 spectrometers (Varian Inc., USA) equipped with a 5-mm Z-SPEC Nalorac IDG 500-5HT gradient probe or a 5-mm PFG AutoXID (^{1}H/X^{15}N-^{31}P) probe, respectively. Samples in CD_2Cl_2 or DMSO-d$_6$ solution were recorded at 25 °C. Standard pulse sequences were used except for the ^{1}H-{^{15}N} correlation. Gradient-enhanced IMPACT-HMBC[3], ^{1}H-{^{15}N} correlation spectra were optimized for a coupling constant of 4 Hz with the following experimental conditions: an acquisition time of 0.2 s, spectral windows of 6000 (F2) and 7600

(F1) Hz, 1231 complex data points in t2, 128 complex data points in t1, 8 or 16 scans per increment, 30 ms WURST-2 mixing sequence centred within the 60 ms preparation interval (ASAP2) and a 140 Ernst angle as the excitation pulse.[4] The data were processed with linear prediction in t1 followed by zero-filling in both dimensions. Gaussian weighting functions were applied in both domains prior to Fourier transformation. All the spectra were referenced according to IUPAC recommendations.[5]

Quantum chemical calculations

All quantum chemical calculations were performed using ORCA 5.0 suite of programs.[6] We used the density functional (DFT) framework with ωB97x-D3 range-separated functional[7] to optimize the geometry of complexes 2-4 in their cationic form. If not stated otherwise, relativistic effects were covered with the DKH2 treatment, and the basis set employed was DKH-def2-TZVP for light atoms and SARC-DKH-TZVP for iridium as implemented in ORCA program.[8] Solvent effects were simulated with CPCM method[9] using parameters of acetonitrile. Whenever possible, we took the advantage of chain-of-spheres approximation[10] to speed-up the calculations (rijcosx in the ORCA nomenclature). In the excited state calculations, we employed the time-dependent DFT approach with Tamm–Dancoff approximation and calculated 50 roots in the singlet and triplet manifolds. The states were allowed to interact via the spin-orbit coupling operator (SOC). The analysis of obtained states involved the identification of key non-relativistic states contributing to the given SOC state, calculating differential densities for this state, and plotting key donor-acceptor orbitals for contributions with high coefficients (c). In this way, the character of the given state was attributed as local or charge-transfer. Non-relativistic calculations in the main text, **Fig. 4d**, were performed with the same basis set as above but with non-relativistic Hamiltonian and without SOC.

Crystal structure determination

The X-ray diffraction data were collected on an IPDS 2T dual-beam diffractometer (STOE&Cie GmbH, Darmstadt, Germany) at 120.0(2) K with Mo-Kα radiation of a microfocus X-ray source (GeniX 3D Mo HighFlux, Xenocs, Sassenage, France, 50 kV, 1.0 mA, λ = 0.71069 Å) for **1-4** structures. Every crystal was thermostated in nitrogen stream at 120 K using CryoStream-800 device (OxfordCryoSystem, UK) during the entire experiment. Data collection and data reduction were controlled by X-Area 1.75 program.[11] The structure was solved by the SHELXT method[12,13] and refined using the program packages Olex2[14,15] and SHELX-2015.[12,13] Diamond[16] was used to prepare the figures. All non-hydrogen atoms were modeled as anisotropic. H-atoms were refined as isotropic. All C-H and N-H type hydrogen atoms were attached at their geometrically expected positions and refined as riding on heavier atoms with the usual constraints. The structure of **3** was refined as an inversion twin. Anion hexafluorophosphate (P1, F1–F6), water molecule and two C atoms (C14 and C16) in **3** were found disordered in two positions with probabilities of 0.645(10)/0.355(10); 0,66(3)/0.34(3) and 0.36(7)/0.64(7), respectively. After the completion of the refinement of **4**, diffuse electron densities were removed from the reflection data by using the SQUEEZE routine of PLATON.[17] The results gave a total potential solvent accessible void volume of 1984 $Å^3$ and a count of 426 electrons, which is in reasonable agreement with the presence of $2[C_2H_6O]$ per asymmetric unit, which account for 416 electrons per unit cell. The crystallographic data and some details of the

structural refinement are summarized in **Table S1**. Crystallographic data for all structures reported in this paper have been deposited with the Cambridge Crystallographic Data Centre as supplementary publication No. CCDC 2234074-2234077. The data can be obtained free of charge from The Cambridge Crystallographic Data Centre via http://www.ccdc.cam.ac.uk/structures.

Table S1 Crystal data and structure refinement for **1-4** complexes.

	1	2	3	4
Empirical formula	$C_{44}H_{44}Cl_2Ir_2N_8$	$C_{67}H_{62}Cl_2F_{12}Ir_2N_{12}O_2P_2$	$C_{28}H_{29}F_6IrN_8OP$	$C_{34}H_{31}F_6IrN_7P$
CCDC number	2234076	2234075	2234077	2234074
Formula weight (g mol^{-1})	1140.17	1812.52	830.76	874.83
Temperature (K)	120(2)	120(2)	120(2)	120(2)
Wavelength (Å)	1.54186	0.71073	0.71073	0.71073
Crystal system, space group	Monoclinic, $C2/c$	Monoclinic, $P2_1/c$	Monoclinic, Pn	Monoclinic, $P2_1/n$
	a = 13.3618(16)	a = 10.4234(5)	a = 12.1393(10)	a = 16.6526(4)
	$\alpha = 90°$	$\alpha = 90°$	$\alpha = 90°$	$\alpha = 90°$
Unit cell dimensions	b = 17.088(2)	b = 20.1866(7)	b = 10.3689(10)	b = 17.3070(3) Å
	$\beta = 99.087(10)°$	$\beta = 105.374(4)°$	$\beta = 97.228(7)°$	$\beta = 93.152(2)°$
	c = 17.841(2)	c = 17.6610(8)	c = 12.5880(11)	c = 27.5369(8) Å
	$\gamma = 90°$	$\gamma = 90°$	$\gamma = 90°$	$\gamma = 90°$
Volume (Å^3)	4022.5(9)	3583.1(3)	1571.9(2)	7924.3(3)
Z	4	2	2	8
Calculated density (Mg m^{-3})	1.883	1.680	1.755	1.467
Absorption coefficient (mm^{-1})	14.185	3.913	4.370	3.469
$F(000)$	2208	1780	814	3440
Theta range for data collection (°)	4.233 to 67.436	2.264 to 29.188	2.197 to 29.150	2.298 to 26.000
	-15<=h<=15	-14<=h<=14	-15<=h<=16	$-19 \leq h \leq 20$
Limiting indices	-20<=k<=16	-27<=k<=27	-14<=k<=14	$-21 \leq k \leq 19$
	-20<=l<=21	-24<=l<=23	-17<=l<=17	$-33 \leq l \leq 33$
Reflections collected / unique	12530 / 3524 [$R_{int} = 0.0303$]	53401 / 9644 [$R_{int} = 0.0290$]	12977 / 7412 [$R_{int} = 0.0283$]	47200 /15532 [$R_{int} = 0.0577$]
Completeness to theta (%)	97.7	99.9	99.7	99.8
Refinement method		Full-matrix least-squares on F^2		
Data / restraints / parameters	3524 / 0 / 256	9644 / 0 / 464	7412 / 2 / 493	15532 / 0 / 892
Goodness-of-fit on F^2	1.156	1.059	1.08	1.062
Final R indices [$I>2\sigma(I)$]	$R_1 = 0.0386$, $wR_2 = 0.1035$	$R_1 = 0.0303$, $wR_2 = 0.0784$	$R_1 = 0.0317$, $wR_2 = 0.0824$	$R_1 = 0.0851$, $wR_2 = 0.2545$
R indices (all data)	$R_1 = 0.0428$, $wR_2 = 0.1097$	$R_1 = 0.0325$, $wR_2 = 0.0802$	$R_1 = 0.0327$, $wR_2 = 0.0832$	$R_1 = 0.1053$, $wR_2 = 0.2711$
Largest diff. peak and hole (e Å^{-3})	1.018 and -1.582	0.895 and -1.758	1.938 and -1.695	3.548 and -2.079

Stability and octanol-water partition coefficient determination

As in the previous work, the behaviour of the complexes in buffer solution (DMSO/buffer) was determined by UV-Vis spectrophotometry and ^1H spectra (DMSO) over time (0 and 24 h or longer).[18] The partition coefficient was determined by the shake-flask method as in previous studies.[18]

Interactions with biomolecules

As indicated previously a protein-free solution of calf thymus DNA (CT-DNA) was prepared in Tris-HCl/NaCl buffer and the concentration was measured from its absorption intensity at 260 nm using the molar absorption coefficient value of 6600 M^{-1} cm^{-1}. The solution

of the ligand or complexes used in the experiments was also prepared in Tris-HCl buffer containing 1% DMSO. In the titration experiments, different concentrations of the CT-DNA was used while the compound analysed was at 15 μM (**2** and **4**) or different concentrations of the complexes were used while concentrations of the CT-DNA was constant (15 μM) (**1** and **3**). The spectra were recorded after solution equilibration for 96 h.

The emission spectra of EB-DNA and the effect of addition of iridium(III) complexes to the equilibrium of EB-DNA ([EB] = 5 μM, [CT-DNA] = 100 μM) was monitored. The concentration of the compounds analysed varied from 0.5 – 10 μM (due to its solubility).

As pointed out earlier bovine serum albumin (BSA) was dissolved in Tris-HCl buffer (pH=7.2) to prepare a stock solution. The concentration of this solution was determined spectrophotometrically using a molar absorption coefficient of 44300 cm^{-1} M^{-1} at 280 nm. In the titration experiments, different molar ratios of complex:BSA were used (0-1.2 μM, [BSA] = 10 μM). The spectra were recorded after solution equilibration for 96 h and the intrinsic equilibrium binding constant (K_b) of the complexes to BSA was obtained by monitoring changes in the absorption intensity according to the Benesi-Hildebrand equation. Interactions of complexes with BSA (3 μM) were confirmed via CD spectra which were recorded in the region of 200-300 nm in a cuvette with a 2 mm path length. The α-helical content of HSA was also calculated according to paper.[19]

Reactions with GSH and NADH

The reaction of analysed complexes (50 μM) with GSH (20 mM) was carried out in TRIS buffer/DMSO mixture (V/V 95:5). The progress of the reaction with 1 h intervals for 24 h was analysed spectrophotometrically.[20] The reaction products of the complexes (0.05 mM) with GSH (0.5 mM) in CH$_3$CN solution were also recorded by ESI-MS.

The reaction of analysed complexes with NADH (molar ratio 1:100) in 50% MeOH/50% H$_2$O was examined by UV-Vis spectroscopy after various time intervals (0.5 - 24 h). TON was calculated from the difference in NADH concentration after 24 h divided by the concentration of analysed iridium complexes. The concentration of NADH was obtained using the extinction coefficient ε_{339} = 6220 M^{-1}cm^{-1}.

Evaluation of cytotoxicity

The effect of 72-hour treatments with the test compounds on cell viability was evaluated using a resazurin reduction assay measuring the metabolic activity of the cell population. The following cell lines were used K-562 (myelogenous leukaemia), CCRF-CEM (acute lymphoblastic leukaemia), MCF-7 (breast cancer), and BJ (skin fibroblasts). They originate from the American Type Culture Collection, Manassas, VA, USA. The cells were maintained in standard DMEM supplemented with fetal bovine serum (10%), glutamine (2 mM), penicillin (100 U/mL) and streptomycin (100 μg/mL) under standard cell culture conditions (37 °C, 5% CO$_2$, humid environment) and subcultured two or three times a week. For the toxicity evaluation, the cells were trypsinized and diluted in DMEM medium. 80 μL of cells in the culture medium were seeded into the wells of a 96-well plate. The inoculum size was 20000 cells for CCRF-CEM, 10000 cells for K-562 and 5000 cells for the other cell lines. After 24 h incubation, the cells were treated with the test compounds

dissolved 20 µL of culture media. Dilution series of six concentrations were tested, each in triplicate. Maximum concentration and dilution were adjusted for the individual compounds, so the obtained measurement values allow IC_{50} concentration calculation for toxic compounds. DMSO vehicle served as a negative control. After 72 hours, 10 µL of 11× concentrated solution of resazurin (Sigma) in the culture medium was added to the cells to the (final concentration of 0.0125 mg/mL). Fluorescence (λ_{ex} = 570 nm, λ_{em} = 610 nm) was measured after 3-hour (other cell lines) incubation using M2 reader (Biotek). Each experiment was repeated at least twice.

Flow cytometric analysis

The effect of the compounds on the cell cycle and apoptosis was evaluated by flow cytometry after 48 hour treatment. About $1x10^6$ CCRF-CEM and $7.5x10^5$ K-562 cells were used for the analysis. The cells were centrifuged (1000 g, 8 min, 4 °C), washed twice in PBS and then fixed in ice cold 70% ethanol and stored at -20 °C before analysis. After rehydratation in PBS, the cells were centrifuged and washed in PBS. The cells were stained with 60 µg/µL propidium iodide (Sigma-Aldrich) for 30 min in dark and then were analysed by on BD FACS VERSE flow cytometer (Becton-Dickinson Company, USA) using BD FACSuite TM Software (Becton-Dickinson Company, USA). Analysis of cell cycle distribution and apoptosis was carried out in ModFit LT 5.0 software (Verity Software House, USA).

a) +MS, 0.1-0.1min #(3-8)

717.209252

719.211309

b) +MS, 0.1-0.2min #(5-13)

667.203950

669.205499

c)
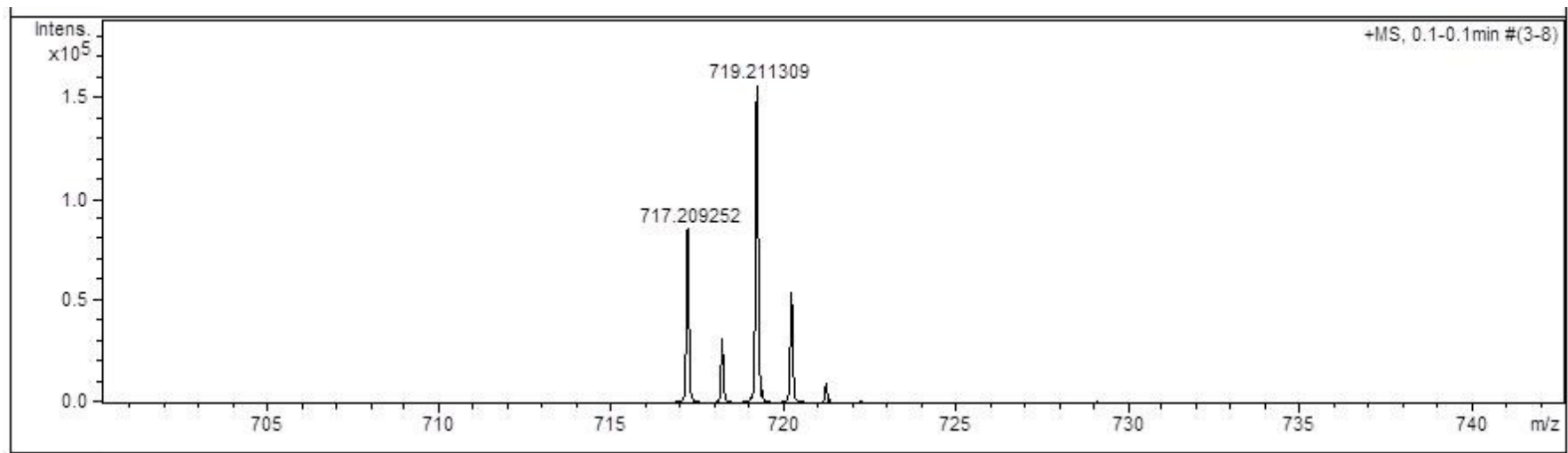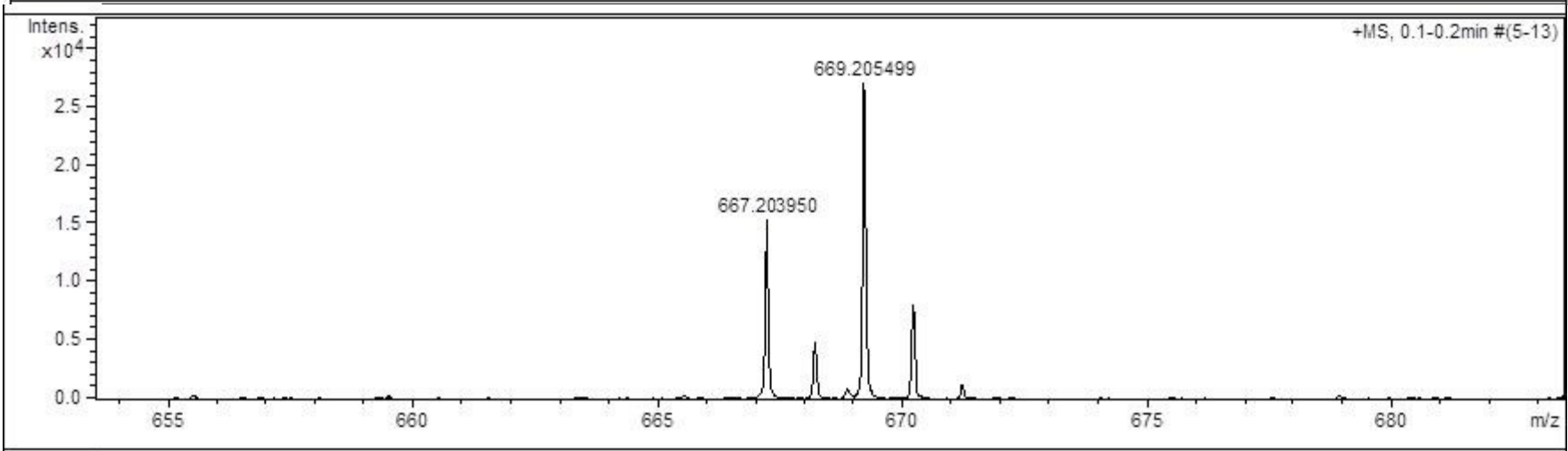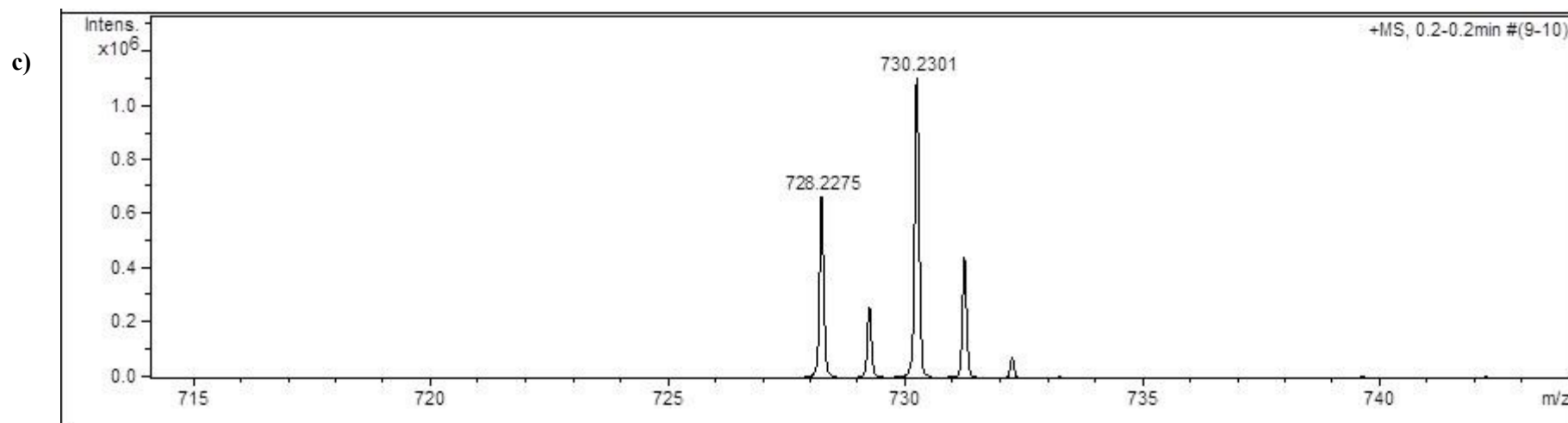
Fig. S1. The ESI-MS spectra of complex a) **2**, b) **3**, c) **4**.

Table S2 Bond lengths [Å] and angles [deg] for **1-4** complexes.

1		2		3		4	
Ir(1)-N(1)	2.036(6)	Ir(1)-N(1)	2.163(3)	Ir(1)-N(1)	2.041(5)	Ir(1)-N(1)	2.043(11)
Ir(1)-N(3)	2.042(6)	Ir(1)-N(2)	2.188(2)	Ir(1)-N(3)	2.037(5)	Ir(1)-N(3)	2.031(11)
Ir(1)-C(1)	2.002(8)	Ir(1)-N(3)	2.038(2)	Ir(1)-N(5)	2.141(5)	Ir(1)-N(5)	2.179(10)
Ir(1)-C(12)	1.995(8)	Ir(1)-N(5)	2.035(2)	Ir(1)-N(7)	2.153(8)	Ir(1)-N(6)	2.139(10)
Ir(1)-Cl(1)	2.5388(15)	Ir(1)-C(22)	2.014(3)	Ir(1)-C(11)	2.007(7)	Ir(1)-C(11)	2.003(14)
Ir(1)-Cl(2)	2.5263(16)	Ir(1)-C(33)	2.009(3)	Ir(1)-C(22)	2.019(6)	Ir(1)-C(22)	2.019(13)
						Ir(2)-N(8)	2.028(11)
						Ir(2)-N(10)	2.011(11)
						Ir(2)-N(12)	2.174(10)
						Ir(2)-N(13)	2.146(10)
						Ir(2)-C(45)	2.008(12)
						Ir(2)-C(56)	2.043(13)
C1(2)-Ir(1)-C(1)	93.8(3)	C(33)-Ir(1)-C(22)	86.73(11)	C(11)-Ir(1)-C(22)	90.1(3)	C(11)-Ir(1)-C(22)	89.5(5)
C1(2)-Ir(1)-N(1)	94.7(3)	C(33)-Ir(1)-N(5)	79.72(11)	C(11)-Ir(1)-N(3)	93.1(3)	C(11)-Ir(1)-N(3)	93.7(5)
C(1)-Ir(1)-N(1)	79.9(3)	C(22)-Ir(1)-N(5)	93.95(11)	C(22)-Ir(1)-N(3)	80.3(3)	C(22)-Ir(1)-N(3)	79.2(4)
C1(2)-Ir(1)-N(3)	80.3(3)	C(33)-Ir(1)-N(3)	92.67(11)	C(11)-Ir(1)-N(1)	80.0(3)	C(11)-Ir(1)-N(1)	78.7(5)
C(1)-Ir(1)-N(3)	91.8(3)	C(22)-Ir(1)-N(3)	79.99(11)	C(22)-Ir(1)-N(1)	92.8(3)	C(22)-Ir(1)-N(1)	94.2(5)

N(1)-Ir(1)-N(3)	170.0(2)	N(5)-Ir(1)-N(3)	170.59(10)	N(3)-Ir(1)-N(1)	170.2(2)	N(3)-Ir(1)-N(1)	170.0(5)
C(12)-Ir(1)-Cl(2)	90.6(2)	C(33)-Ir(1)-N(1)	95.39(11)	C(11)-Ir(1)-N(5)	95.8(3)	C(11)-Ir(1)-N(6)	172.8(4)
C(1)-Ir(1)-Cl(2)	175.5(2)	C(22)-Ir(1)-N(1)	177.59(11)	C(22)-Ir(1)-N(5)	174.1(3)	C(22)-Ir(1)-N(6)	97.6(4)
N(1)-Ir(1)-Cl(2)	98.35(17)	N(5)-Ir(1)-N(1)	85.31(10)	N(3)-Ir(1)-N(5)	99.6(2)	N(3)-Ir(1)-N(6)	86.5(4)
N(3)-Ir(1)-Cl(2)	90.35(17)	N(3)-Ir(1)-N(1)	101.02(10)	N(1)-Ir(1)-N(5)	88.0(3)	N(1)-Ir(1)-N(6)	101.8(5)
C1(2)-Ir(1)-Cl(1)	172.0(2)	C(33)-Ir(1)-N(2)	176.50(11)	C(11)-Ir(1)-N(7)	172.3(3)	C1(1)-Ir(1)-N(5)	96.0(4)
C(1)-Ir(1)-Cl(1)	94.1(2)	C(22)-Ir(1)-N(2)	89.91(10)	C(22)-Ir(1)-N(7)	97.5(4)	C(22)-Ir(1)-N(5)	174.3(4)
N(1)-Ir(1)-Cl(1)	88.00(17)	N(5)-Ir(1)-N(2)	99.55(10)	N(3)-Ir(1)-N(7)	86.4(3)	N(3)-Ir(1)-N(5)	102.0(4)
N(3)-Ir(1)-Cl(1)	98.11(17)	N(3)-Ir(1)-N(2)	87.71(10)	N(1)-Ir(1)-N(7)	101.4(3)	N(1)-Ir(1)-N(5)	85.4(4)
Cl(2)-Ir(1)-Cl(1)	81.60(6)	N(1)-Ir(1)-N(2)	87.95(10)	N(5)-Ir(1)-N(7)	76.6(3)	N(6)-Ir(1)-N(5)	77.0(4)
						C(45)-Ir(2)-N(10)	94.9(5)
						C(45)-Ir(2)-N(8)	79.4(5)
						N(10)-Ir(2)-N(8)	173.0(4)
						C(45)-Ir(2)-C(56)	88.6(5)
						N(10)-Ir(2)-C(56)	80.4(5)
						N(8)-Ir(2)-C(56)	95.3(5)
						C(45)-Ir(2)-N(13)	98.3(4)
						N(10)-Ir(2)-N(13)	99.5(4)
						N(8)-Ir(2)-N(13)	85.4(4)
						C(56)-Ir(2)-N(13)	173.1(4)
						C(45)-Ir(2)-N(12)	173.8(5)
						N(10)-Ir(2)-N(12)	86.9(4)
						N(8)-Ir(2)-N(12)	99.2(4)
						C(56)-Ir(2)-N(12)	97.6(4)
						N(13)-Ir(2)-N(12)	75.6(4)

Table S3 Hydrogen bonds and inter- or intramolecular interactions for **1-4** [Å and deg.].

D-H···A	d(D-H)	d(H···A)	d(D···A)	<(DHA)
1				
C(10)-H(10A)···Cl(2)	0.98	2.75	3.3148(8)	117.2
C(10)-H(10C)···Cg1[#1]	0.98	2.68	3.6519(9)	169.0
C(2)[#1]-H(2)[#1]···Cg1[#1]	0.95	2.79	3.5572(7)	138.0
C(21)[#1]-H(21)[#1]···Cg2	0.98	2.65	3.5898(8)	160.5
C(22)[#2]-H(22C)[#2]···Cg3	0.98	2.67	3.413(1)	133.2
2				
C(37)-H(37A)···Cl(2)[#1]	0.99	2.88	3.6009(2)	130.7

C(16)#2-H(16A)#2 ···O(1)	0.98	2.45	3.3422(5)	151.3
C(15)-H(15A) ···O(1)	0.98	2.67	3.560(5)	151.4
C(16)-H(16C) ···F(4)#3	0.98	2.45	3.3745(5)	157.5
C(18)-H(18C) ···F(4)#3	0.95	2.48	3.2013(4)	132.4
C(35)#4-H(35)#4 ···F(4)#3	0.95	2.47	3.1451(4)	127.8
C(9)-H(9) ···F(1)	0.95	2.45	3.1514(5)	130.3
C(9)-H(9) ···F(5)	0.95	2.28	3.2246(5)	171.6
3				
N(8)-H(8A) ···O(1)	0.88	1.7946(10)	2.6293(17)	157.5
N(6)-H(6)···O(1)	0.88	2.3942(17)	3.1152(20)	139.4
N(8)-H(8A) ···O(2)	0.88	2.2012(17)	3.0737(22)	171.3
N(6)-H(6)···F(3)#1	0.88	2.3540(12)	2.9377(12)	124.0
C(16)-H(16E) ···F(4A)	0.98	2.2288(32)	2.9499(65)	129.6
C(16)-H(16E) ···F(6A)	0.98	2.5472(32)	3.5168(63)	171.4
C(24)-H(24) ···F(6A)	0.95	2.5110(31)	3.3358(31)	145.2
C(5)-H(5B) ···F(3A)	0.98	2.5239(22)	3.3173(26)	137.9
4				
C(30)-H(30)···Cg1	0.95	2.8080(1)	3.7104(12)	158.8
C(30)-H(30)···Cg2	0.95	2.9107(1)	3.5866(14)	129.2
C(31)-H(31)···Cg3	0.95	2.5649(1)	3.4563(13)	156.5
C(64)-H(64)···Cg4	0.95	2.9282(1)	3.8247(13)	157.8
C(18)-H(18) ···F(2)#1	0.95	2.5961(2)	3.4019(23)	143.0
C(41)-H(41) ···F(9)#2	0.95	2.6622(2)	3.4271(22)	138.0
C(67)-H(67) ···F(3)#3	0.95	2.3940(2)	3.2999(2)	159.5
N(7)-H(7A)···F(8)#4	0.86	2.0707(1)	2.9181(2)	168.3
C(39)#1-H(39C)#1···Cg2	0.98	2.7705(1)	3.4024(2)	122.8
C(5)#1-H(5C)#1···Cg3	0.98	2.6677(1)	3.4755(2)	140.1

Symmetry transformations used to generate equivalent atoms: (**1**) #1 1-x, y, 0.5-z, #2 0.5-x, 1.5-y, 1-z; (**2**) #1 2-x, 1-y, 2-z, #2 x, 1.5-y, -0.5+z, #3 2-x, 1-y, 1-z, #4 1-x, 0.5+y, 0.5-z, (**3**) #1 -0.5+x, 1-y, -0.5+z; #2 -0.5+x, 2-y, 0.5+z; (**4**) #1 0.5-x, -0.5+y, 1.5-z; #2 1.5-x, 0.5+y, 1.5-z; #3 1-x, 2-y, 2-z; #4 -1+x, y, z;
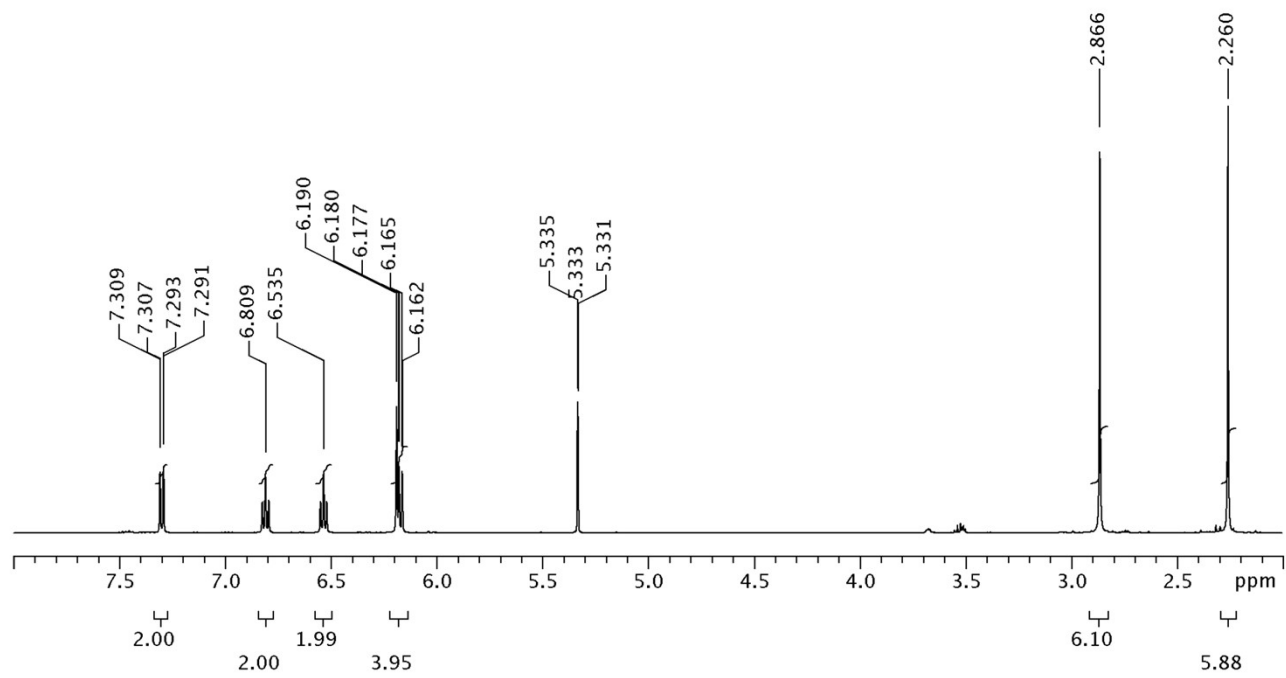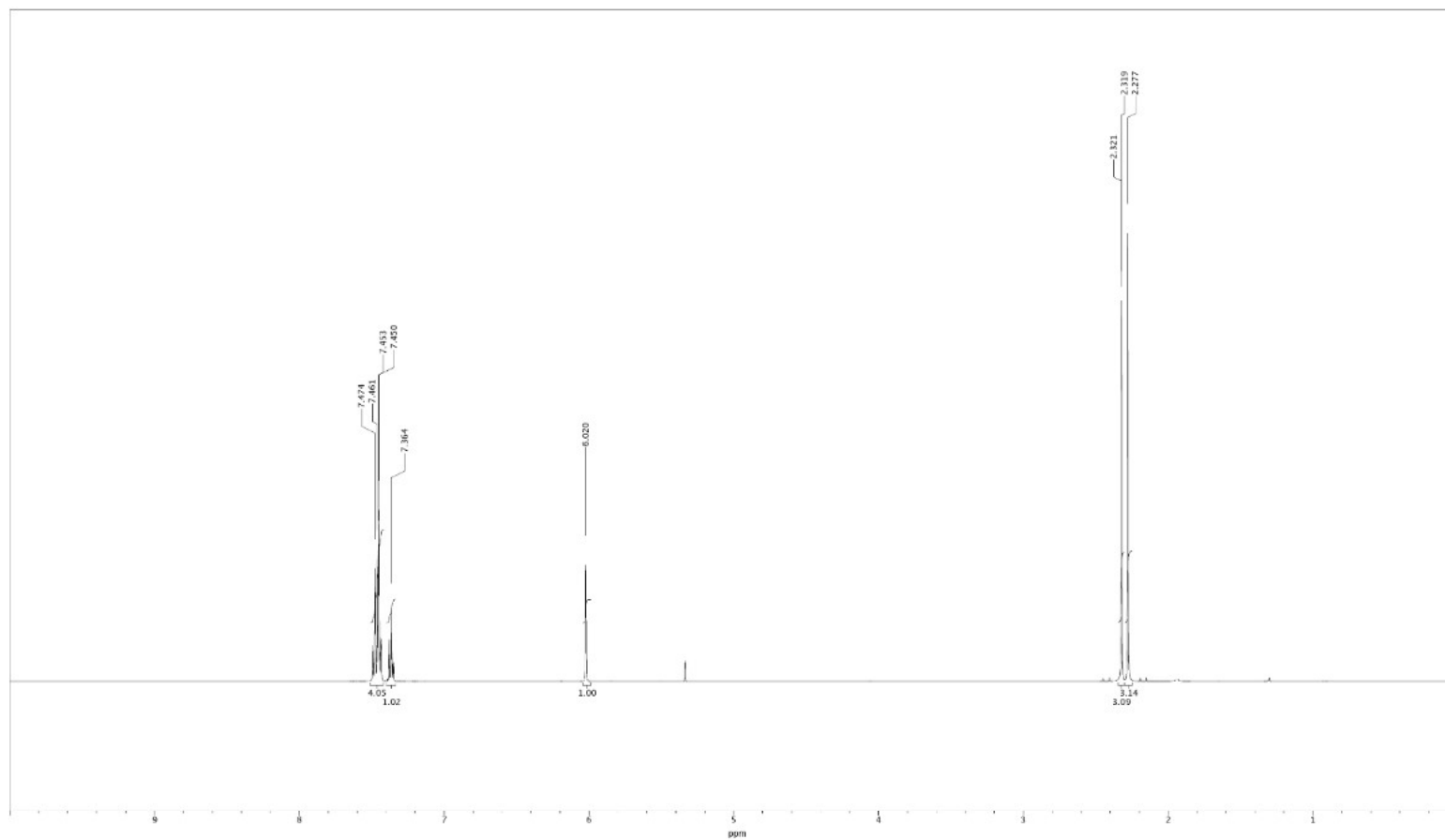
Fig. S2 ^{1}H NMR spectrum of **1** and Hdmppz in CD$_2$Cl$_2$ solution
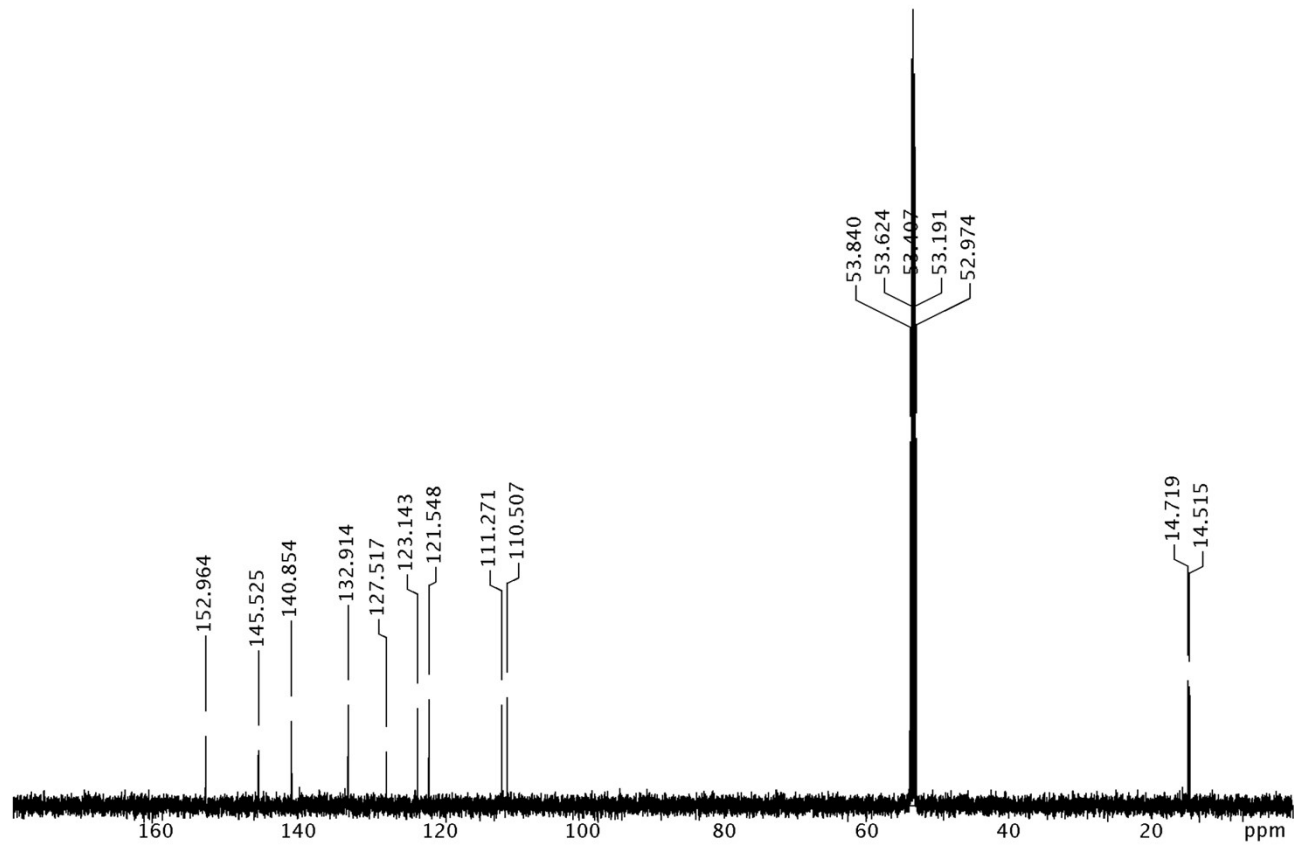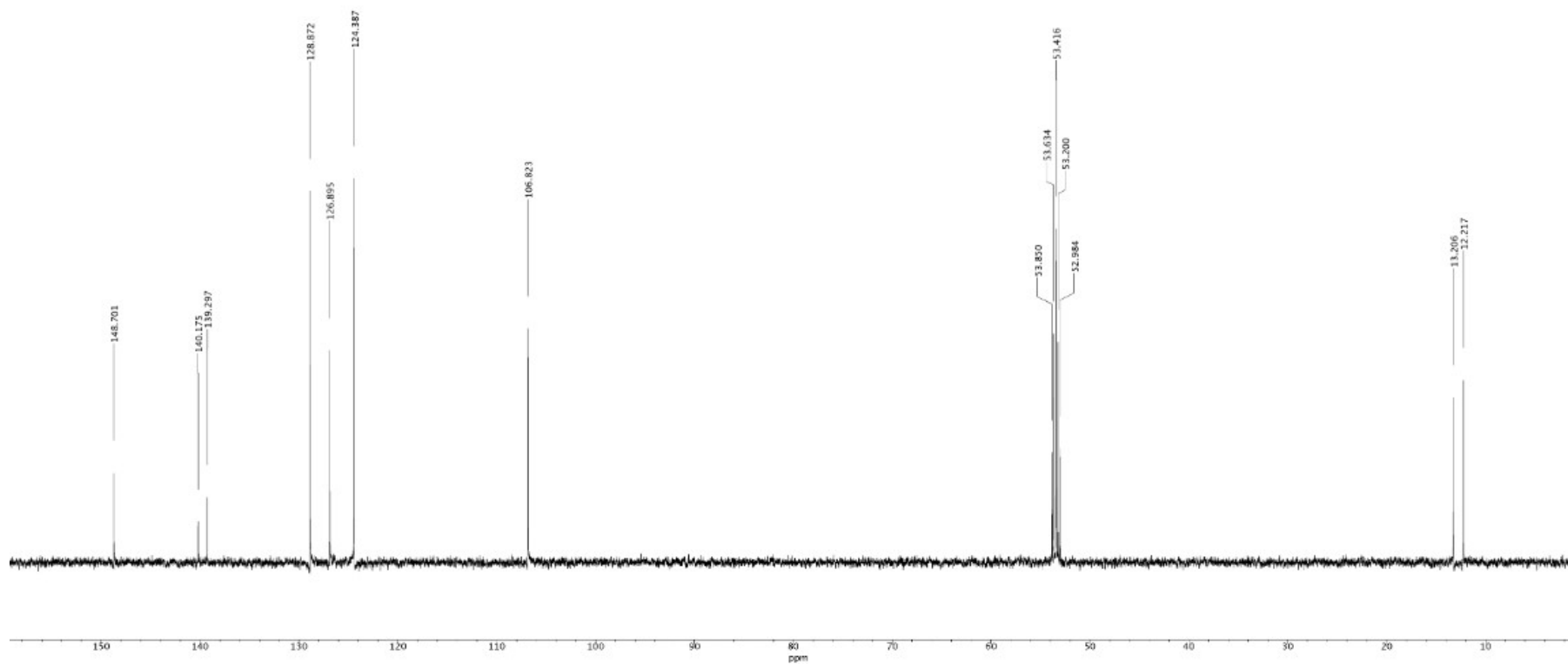
Fig. S3 ^{13}C NMR spectrum of **1** and Hdmppz in CD$_2$Cl$_2$ solution
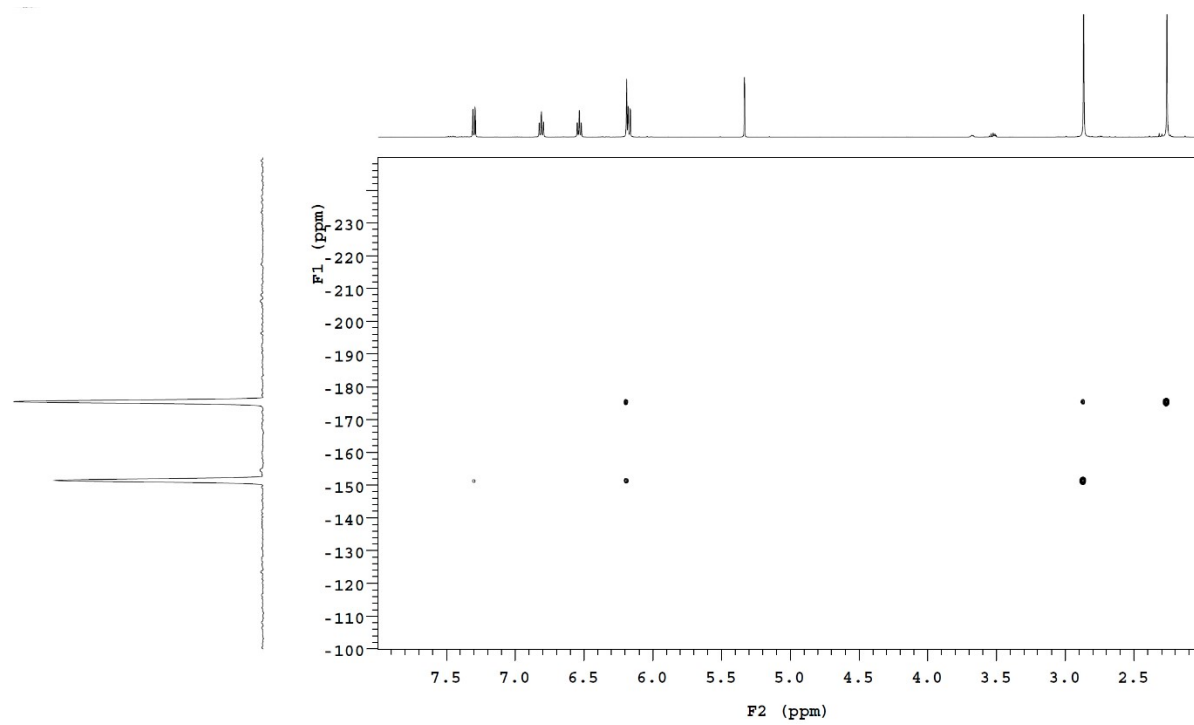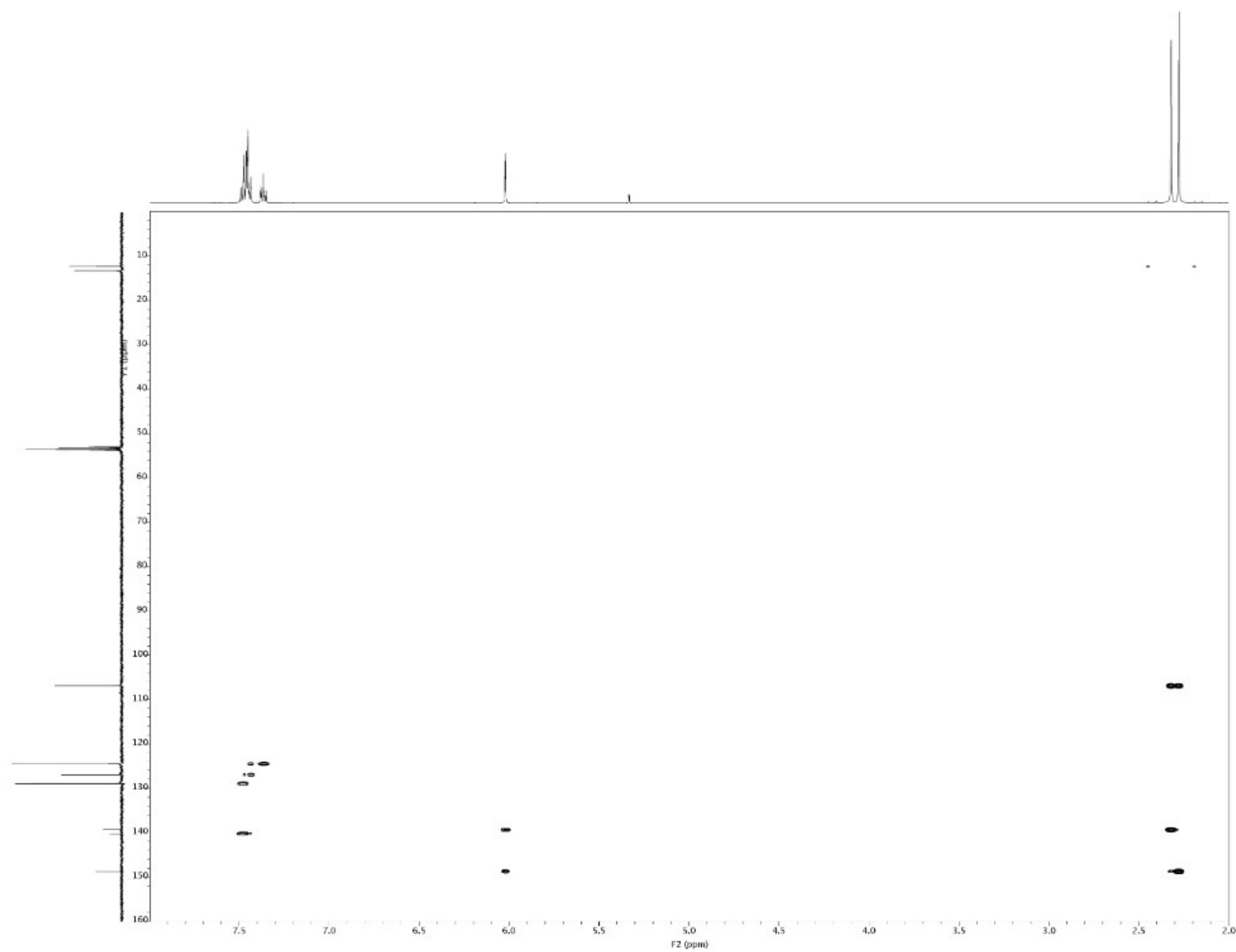
Fig. S4 ^{1}H-^{15}N HMBC NMR spectrum of **1** and Hdmppz in CD$_2$Cl$_2$ solution

15
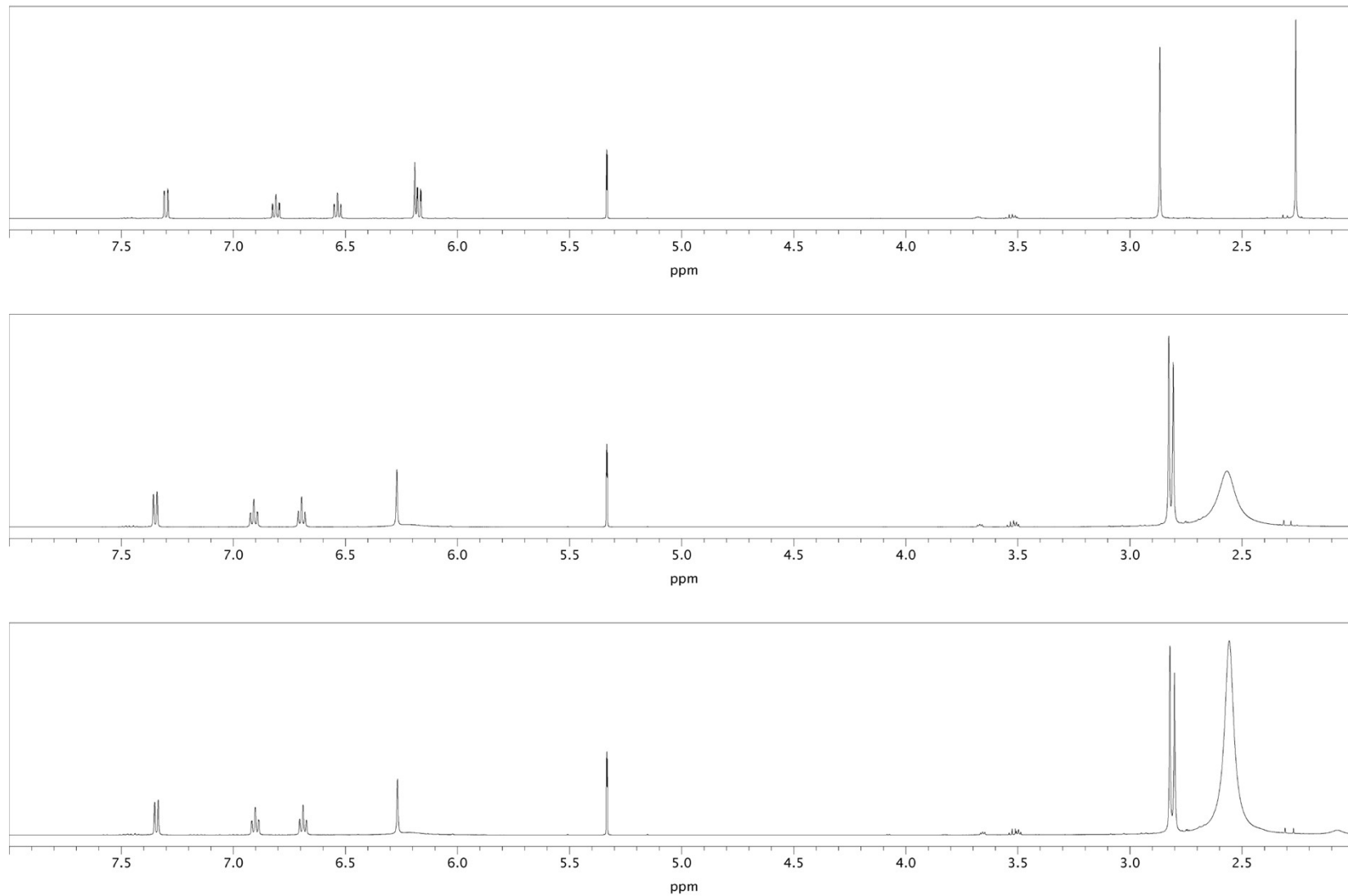
Fig. S5 ^{1}H NMR spectrum of **1** in CD$_2$Cl$_2$ solution spiked with 5 and 10 μL of DMSO.

a)   b)
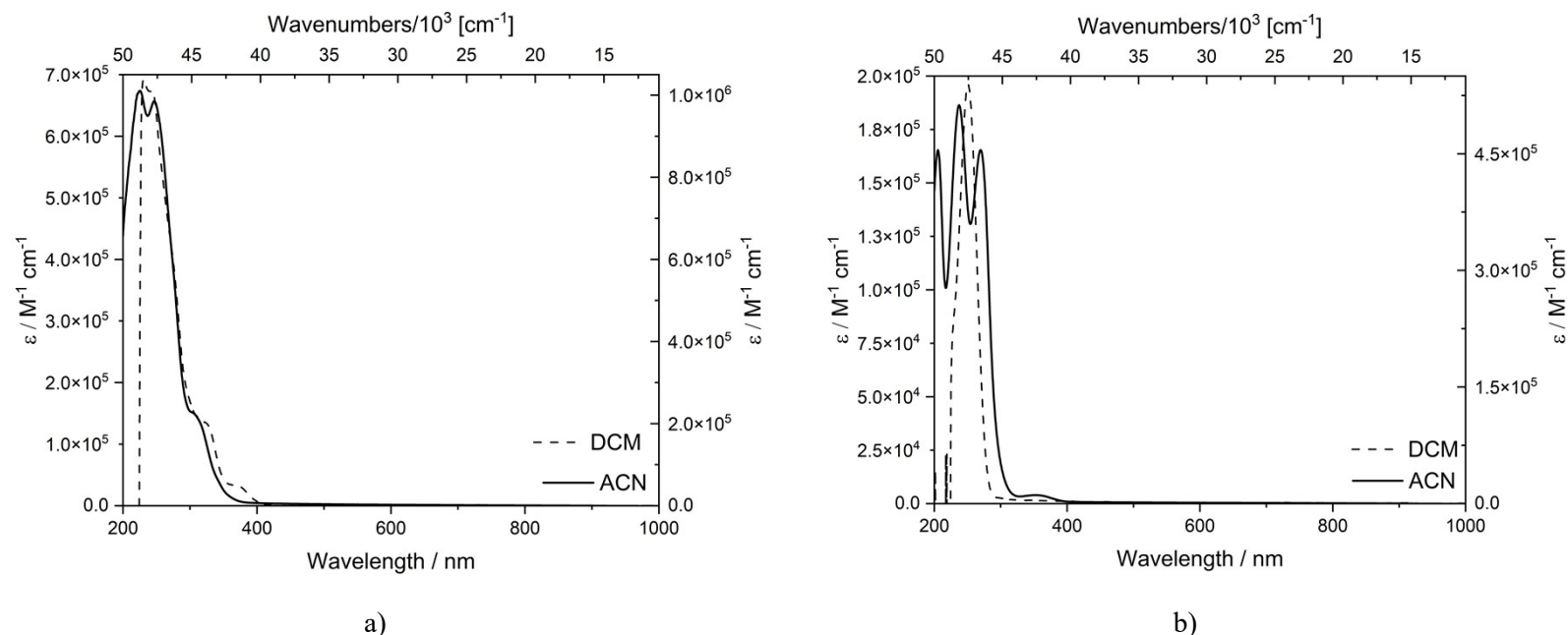
Fig. S6 Absorption spectra of dimer **1** (a) and free ligand Hdmppz (b) in DCM (CH$_2$Cl$_2$) (---) and ACN (CH$_3$CN) (—) solution at room temperature.

Table S4 Electronic absorption parameters for complexes **1-4** and free ligands in CH$_2$Cl$_2$ and CH$_3$CN.

Compound	**1**	Hdmppz	**2**	Py$_2$CO	**3**	H$_2$biim	**4**	PyBIm
CH$_2$Cl$_2$								
λ_{abs}/nm (log ε)	231 (6.01), 243 (6.00), 325 (5.30), 373 (4.68)	251 (5.73)	229 (5.58), 250 (5.55), 352 (4.56), 510 (4.07)	239 (5.02), 272 (4.50), 357 (3.11)	230 (4.57), 255 (4.57), 281 (4.44)	209 (3.77), 277 (2.53)	207 (4.15), 219 (4.22), 247 (3.30), 323 (2.87)	240 (3.55), 310 (3.90), 323 (3.81)
CH$_3$CN								
λ_{abs}/nm (log ε)	225 (5.82), 247 (5.81), 306 (5.17)	206 (5.12), 237 (5.27), 259 (5.22)	214 (5.51), 252 (5.44), 345 (4.49), 487 (4.02)	218 (5.81), 239 (5.93)	207 (4.75), 251 (4.62), 295 (4.32), 353 (3.65)	208 (2.7), 272 (3.20), 278 (3.18), 291 (2.87)	211 (3.78), 240 (3.64), 322 (3.35), 360 (3.07)	220 (4.26), 238 (4.11), 308 (4.47), 319 (4.38)

We would like to mention that the d-d bands for complexes **2** and **4** corresponding to the $^3T_{1g}\leftarrow{}^1A_{1g}$ transition for the d^6 electron ion Ir(III) (ground state ^{1}I)) and in octahedral complexes ($^1A_{1g}(t_{2g}^6)$) are spin-forbidden and according to the Laporte rule. But at the same time the lowest lying spin triplet transition may be obscured by charge transfer absorption. Their intensities are rather high for spin forbidden bands, because the large spin orbit coupling coefficient causes significant mixing of spin states.[21]

The thermal stability of the selected complexes was carried out and the results is shown in **Fig. S7** and **Table S5**.

The first weight loss from 30 to 364 °C is owing to liberation of CH_2Cl_2, counterions with a methyl group of dmppz⁻ ligand from complex **2**. The second weight loss occurs when temperature increases above 364 °C where complex begin to dissociate, which can be assigned to the thermal release of Py_2CO and two cyclometalated ligands. The calculated mass of the thermal decomposition residue of complex **2** indicates a compound with the formula $Ir+N_2$.

The desolvation process of the water molecule in complex **3** occurs in a single narrow step (from 180 to 220 °C). Then we can observe a gradual decomposition of the organic fragments of the complex up to 788 °C with $Ir+N_2$ as the final product.

At the same time, the final step of compound decomposition confirms the high stability of the shortest Ir-N bonds originating from the cyclometalating ligand in the structure of the complexes.

a)   b)
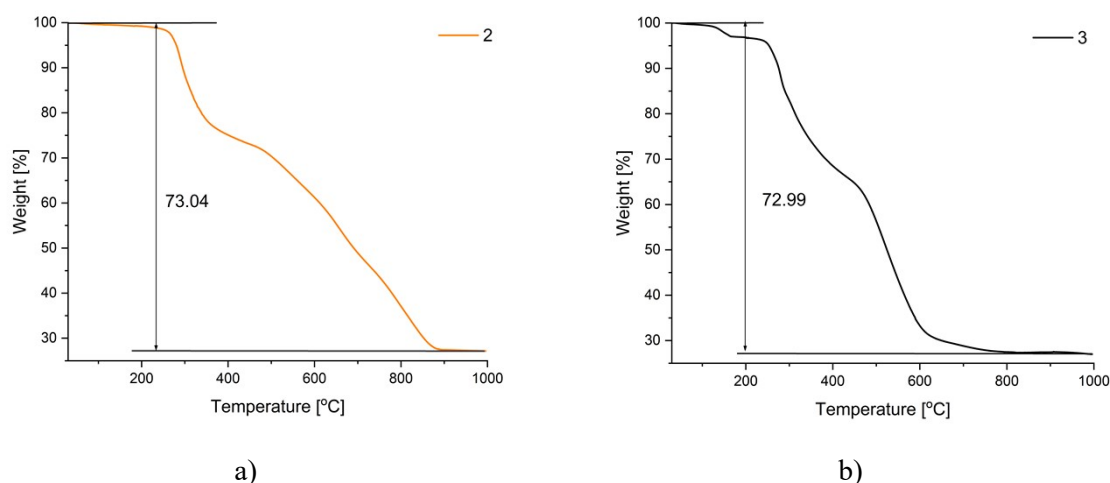
Fig. S7 TG curves for decomposition of complexes (a) **2** and (b) **3**.

Table S5 Thermogravimetric results for complexes **2** and **3**.

Complex	Stage	T_{range} (°C)	Mass (%)		Loss	Residue
			Calc.	Found		
2	I	30-364	23.99	23.12	½ CH_2Cl_2, PF_6^-, 0.17 dmppz⁻	
	II	364-892	48.79	49.72	Py_2CO, 1.67 dmppz⁻	
	Σ		72.78	72.84		
			27.22	27.16		$Ir+N_2$
3	I	180-220	2.17	2.71	H_2O	
	II	220-400	27.33	27.25	PF_6^-, 0.61 H_2biim	
	III	400-788	44.35	43.03	0.39 H_2biim, 1.84 dmppz⁻	
	Σ		73.85	72.99		
			26.15	27.01		$Ir+N_2$
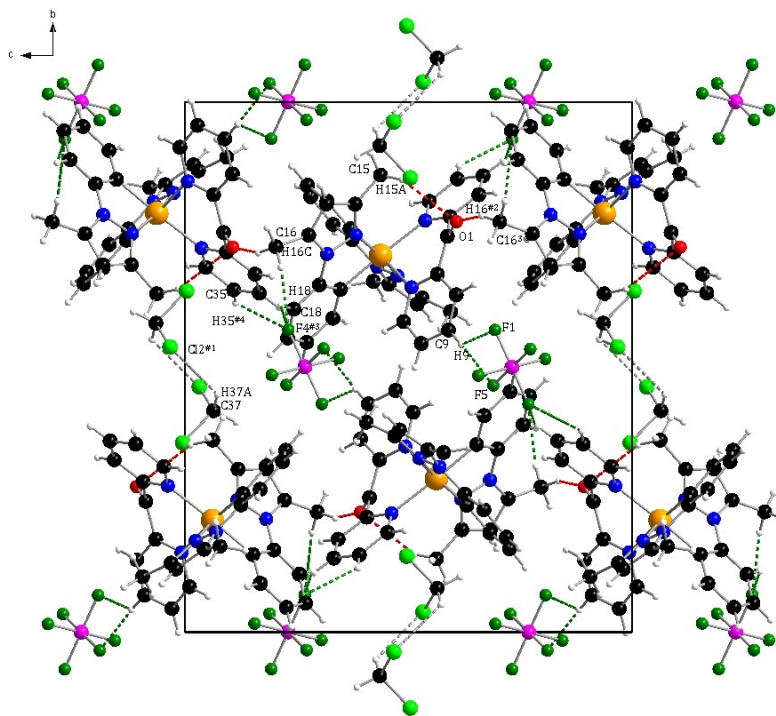
a)
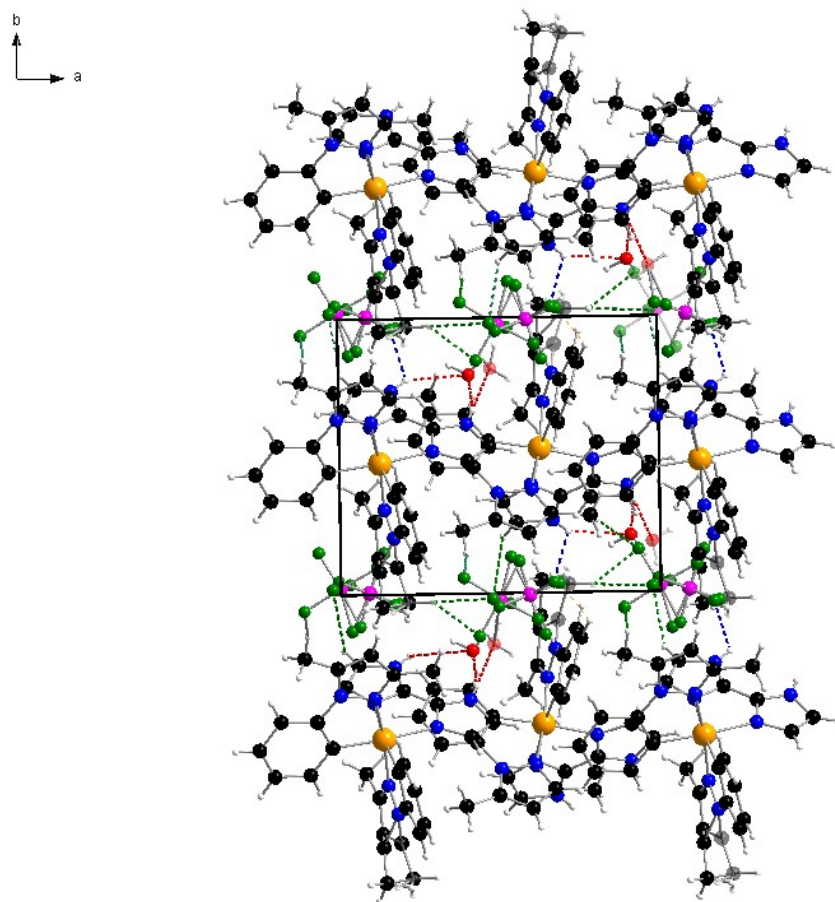
b)
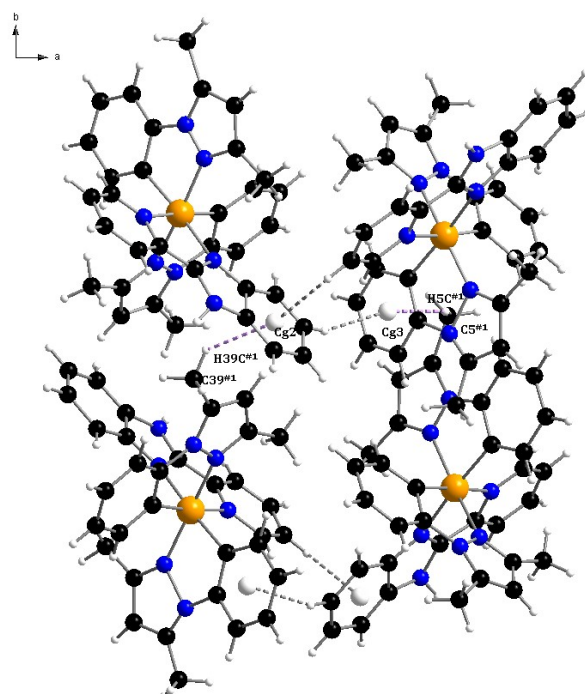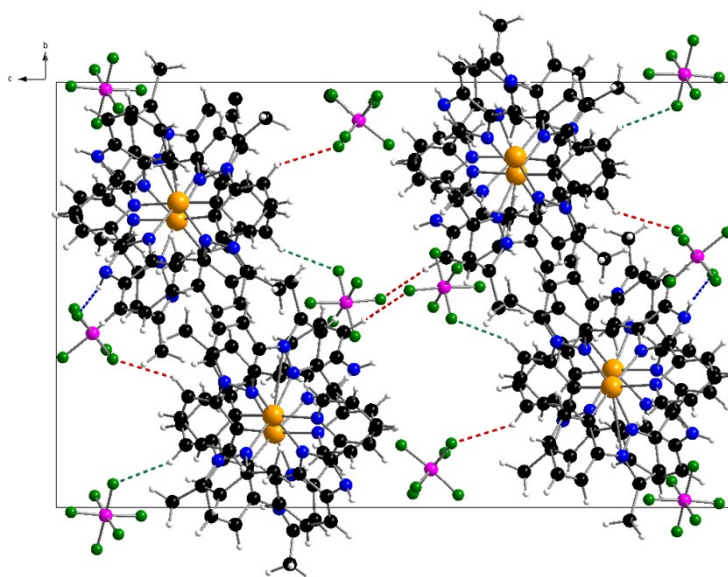
c)

Fig. S8 Packing diagrams of complexes (a) **2**, (b) **3** and (c) **4** showing noncovalent interactions (types: C-H···F/O/Cl, N-H···F) with additional intermolecular C-H···π interactions for complex **4**.
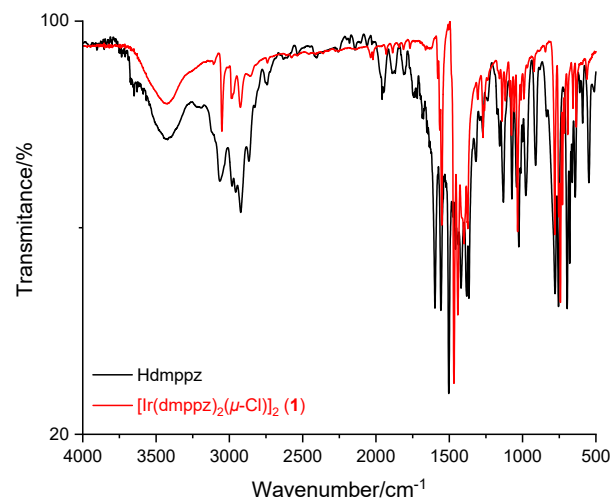
a)
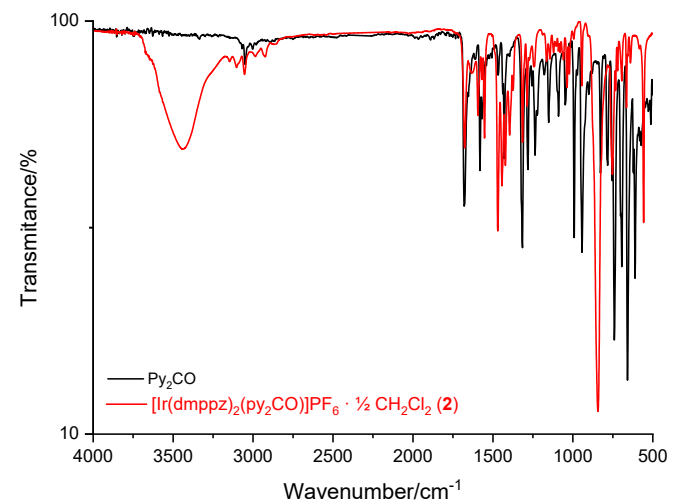
b)
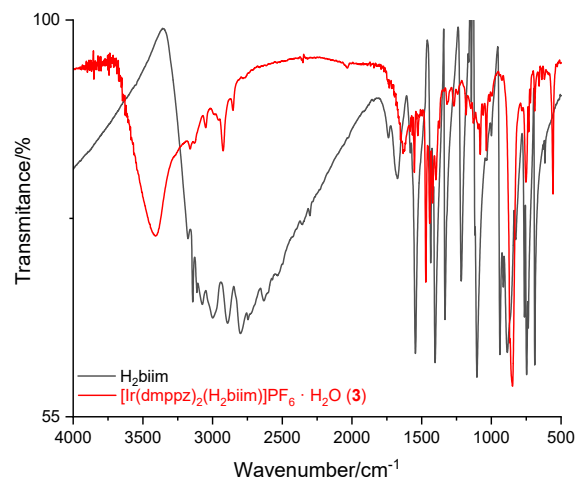
c)
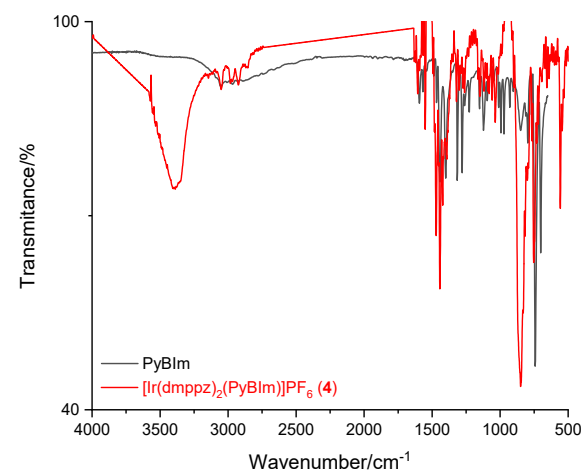
d)

Fig. S9 Experimental FT-IR spectra of free ligands (black) and complexes **1-4** (red).

Table S6 The selected assignments for FT-IR spectroscopic data of free ligands and complexes **1-4**.

Compound	Assignments [cm⁻¹]							
	ν(O-H)	ν(N-H)	ν(C-H)	ν(C=O)	ν(C=C)	ν(C=N)	ν(N-N)	ν(P-F)
Hdmppz	-	-	$3065_{(ar)}$, $2922_{(CH3)}$	-	1598, 1558, 1503, 1474	1438	1026	-
1	-	-	$3052_{(ar)}$, $2925_{(CH3)}$	-	1579, 1565, 1551, 1470	1443	1035	-
Py_2CO	-	-	$3094_{(ar)}$	1679	1581, 1568, 1467	1429	-	-
2	3442		$3054_{(ar)}$	1677	1594, 1568, 1553, 1470	1444, 1422	1036	843
H_2biim	-	3132	-	-	1545	1435	-	-
3	3411	-	$2924_{(CH3)}$	-	1552	1443, 1422	1036	849
PyBIm	-	3057	-	-	1594, 1568, 1540	1443, 1401	-	-
4	3388	-	$3051_{(ar)}$, $2925_{(CH3)}$	-	1605, 1551, 1470	1443, 1422	-	850
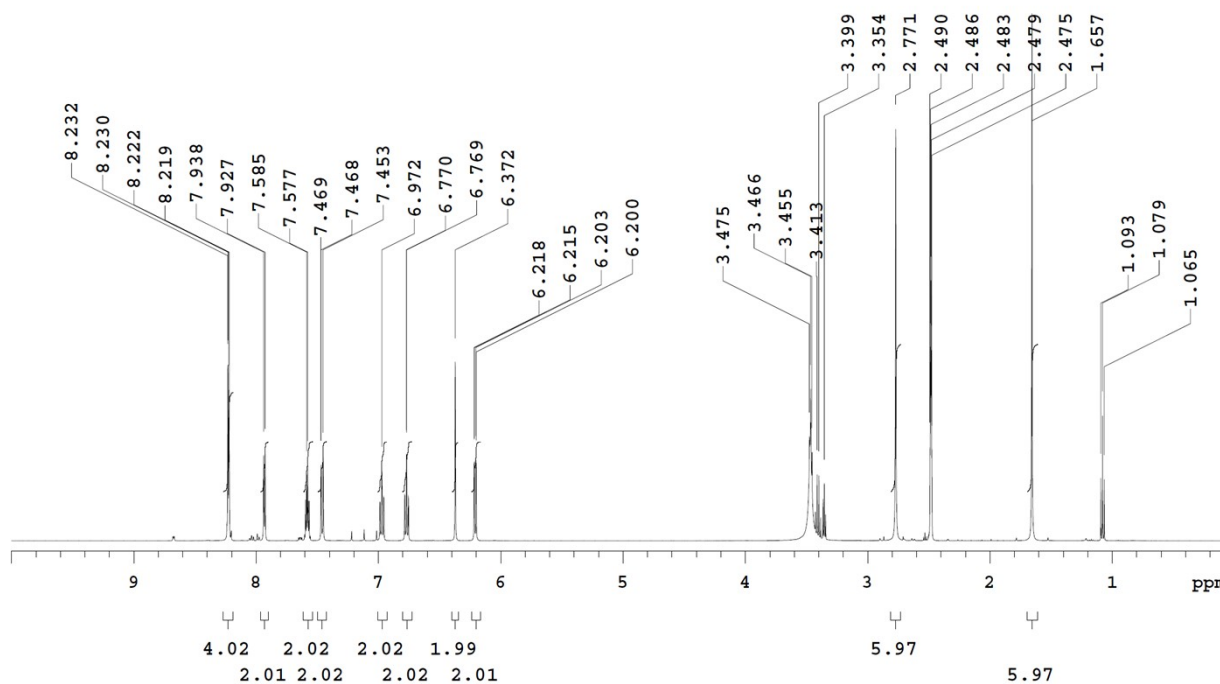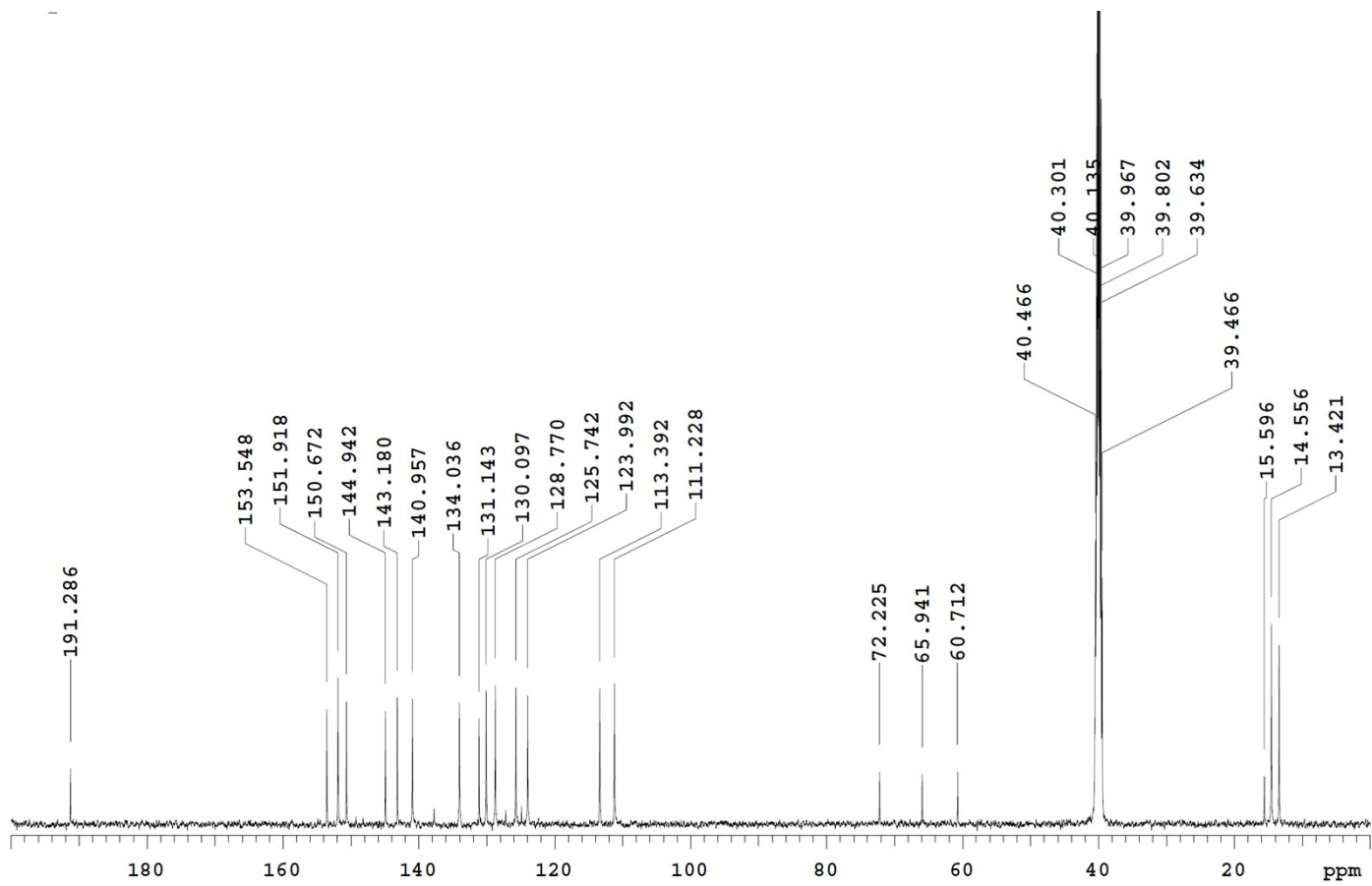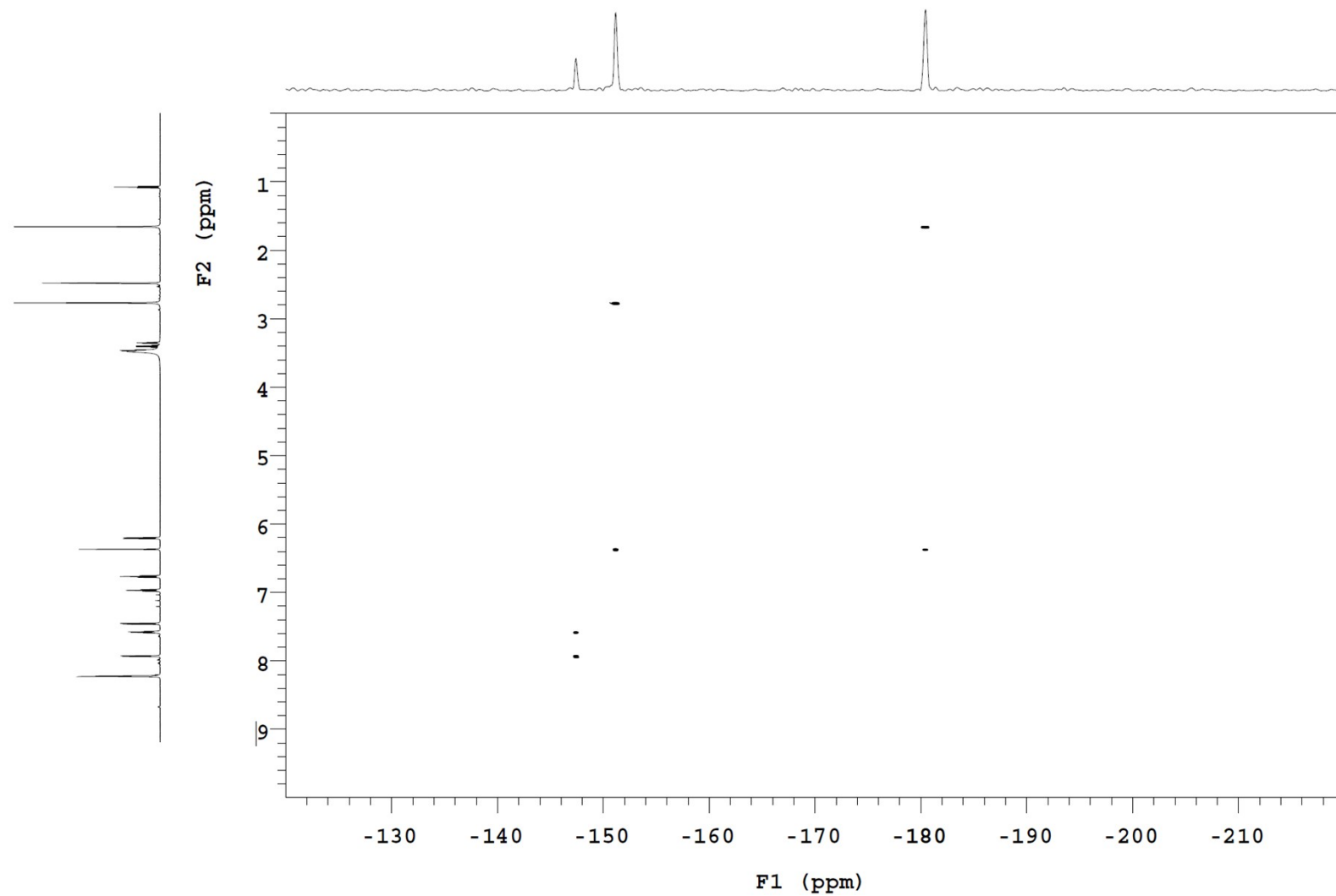
Fig. S10 ^{1}H, ^{13}C and ^{1}H-^{15}N HMBC NMR spectrum of **2** in DMSO-d$_6$ solution
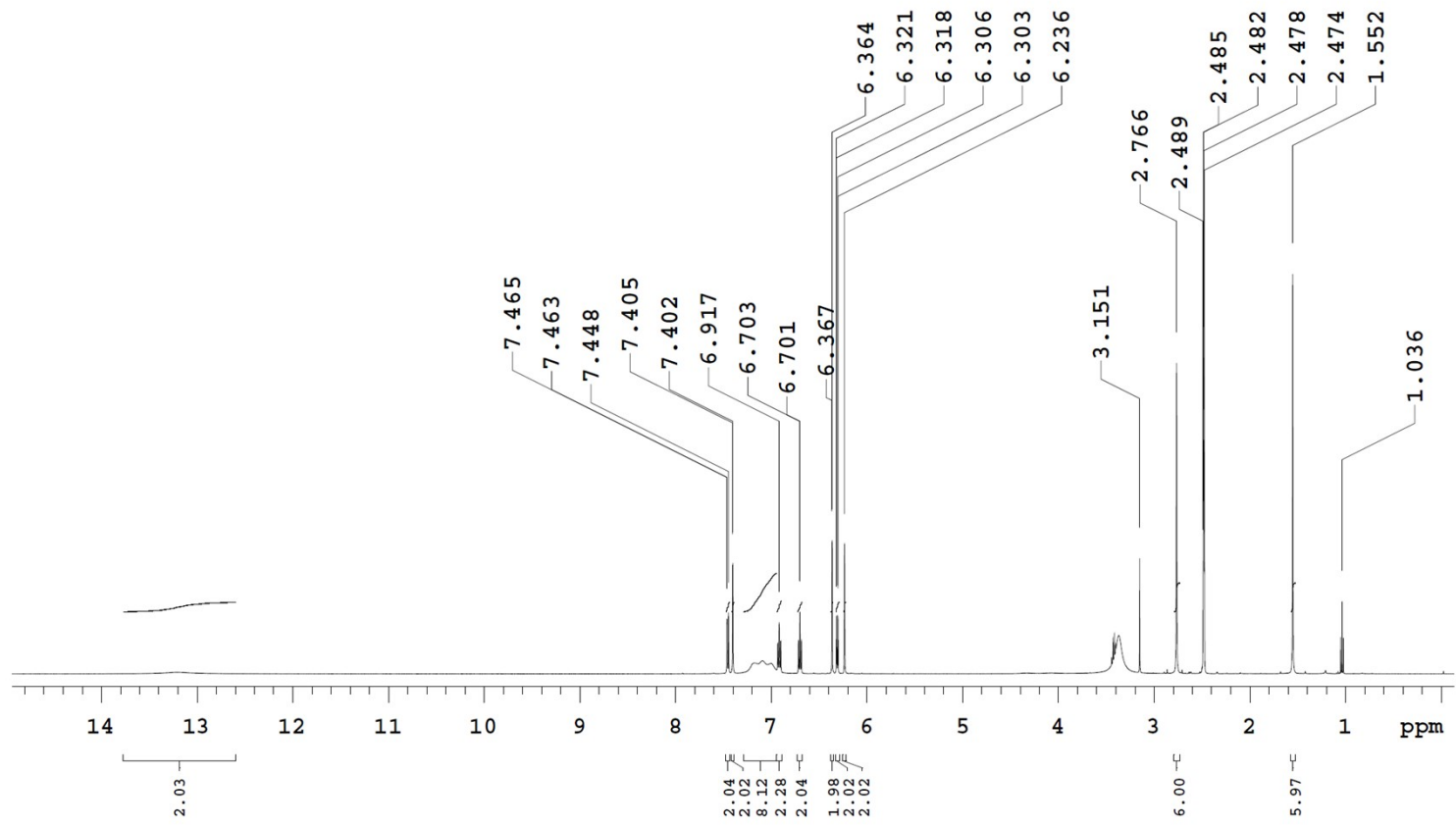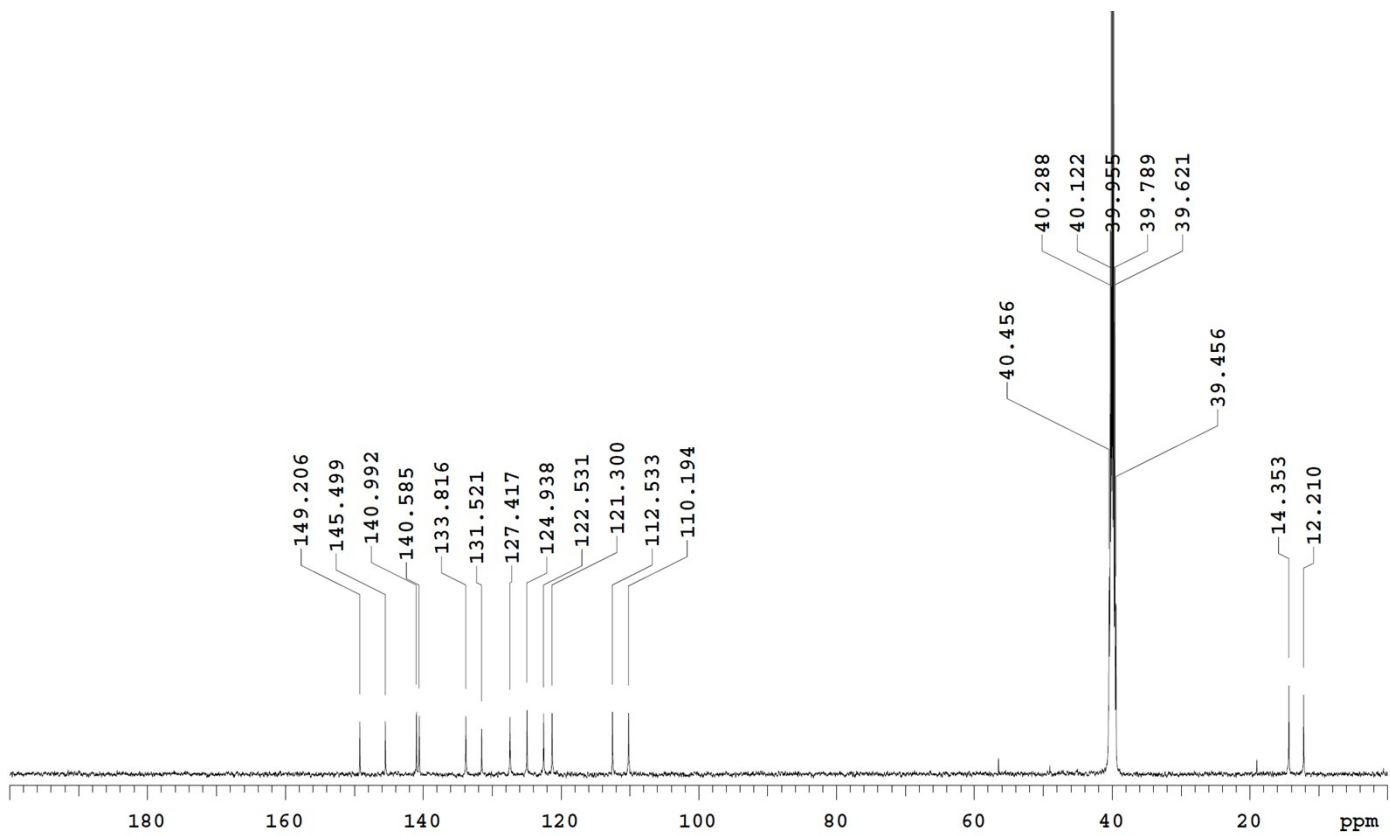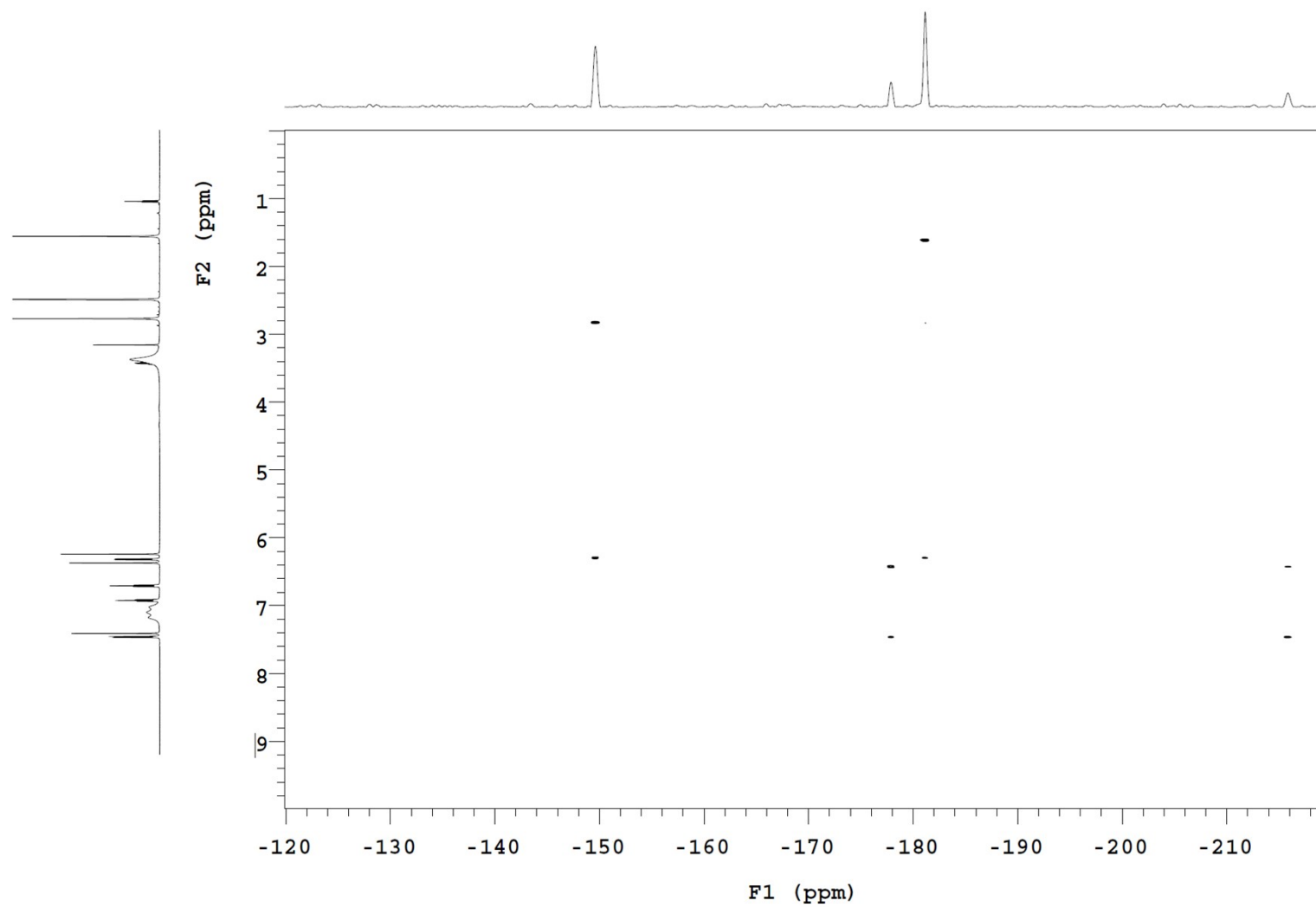
Fig. S11 ^{1}H, ^{13}C and ^{1}H-^{15}N HMBC NMR spectrum of **3** in DMSO-d$_6$ solution

29
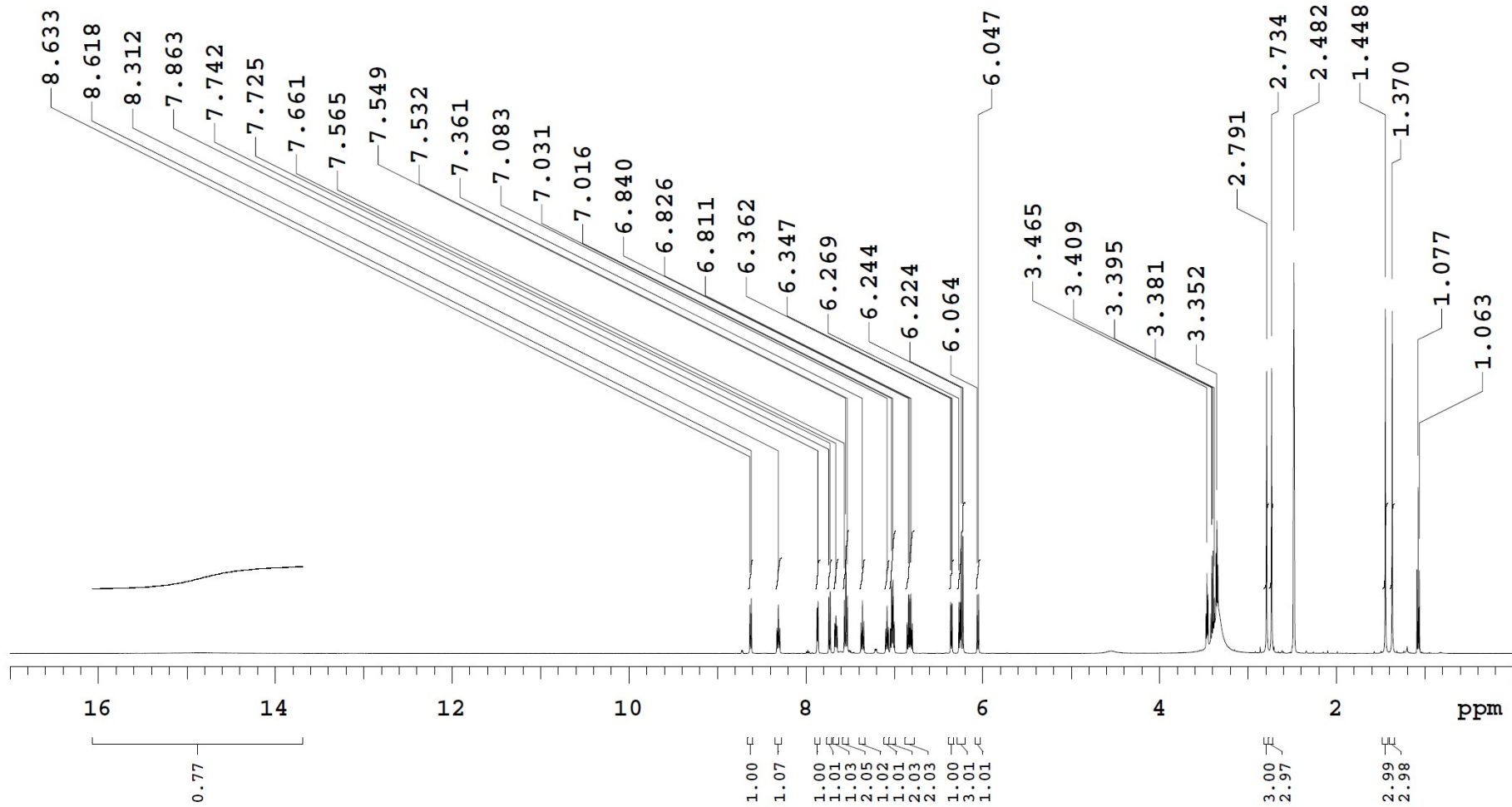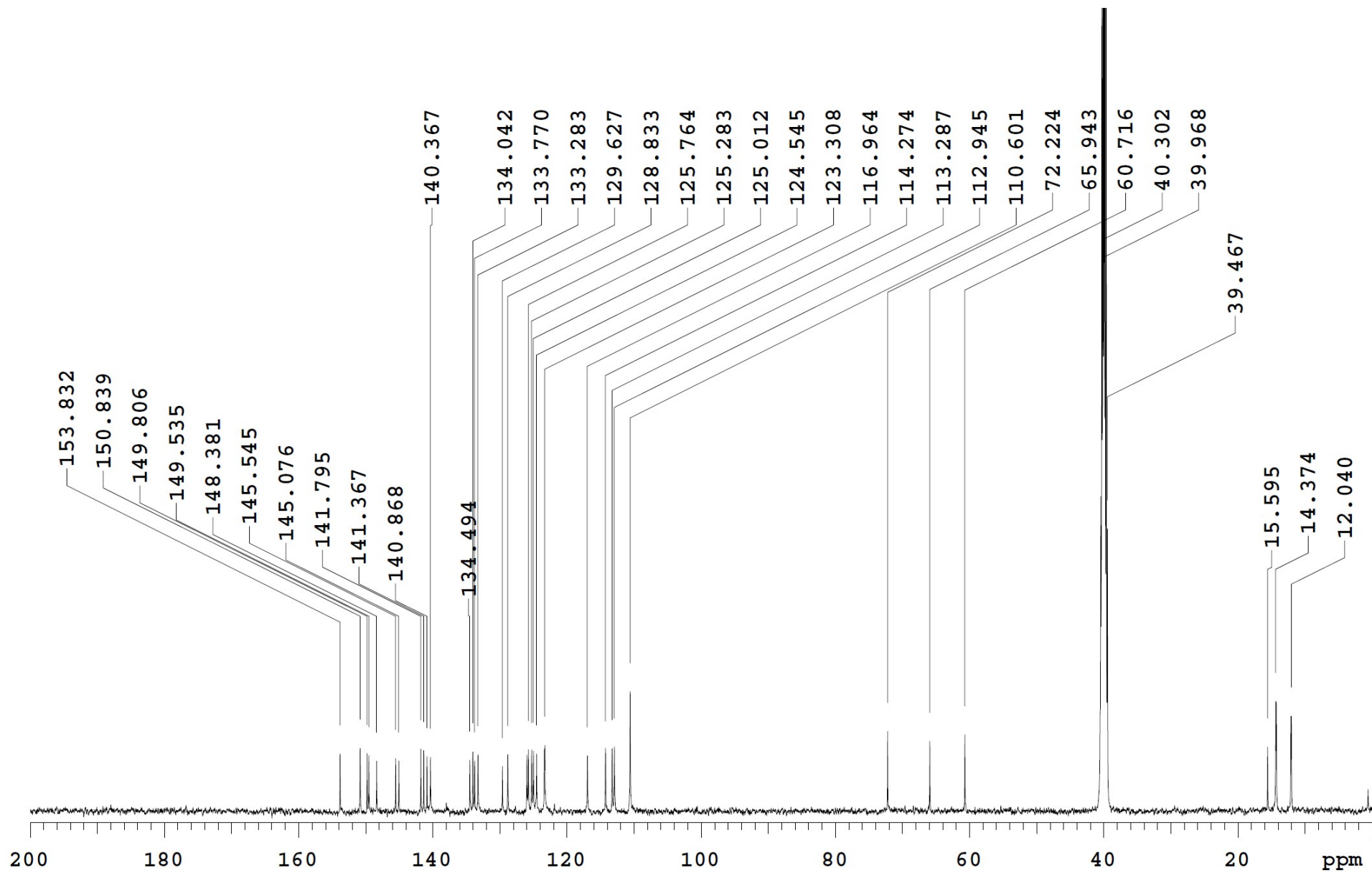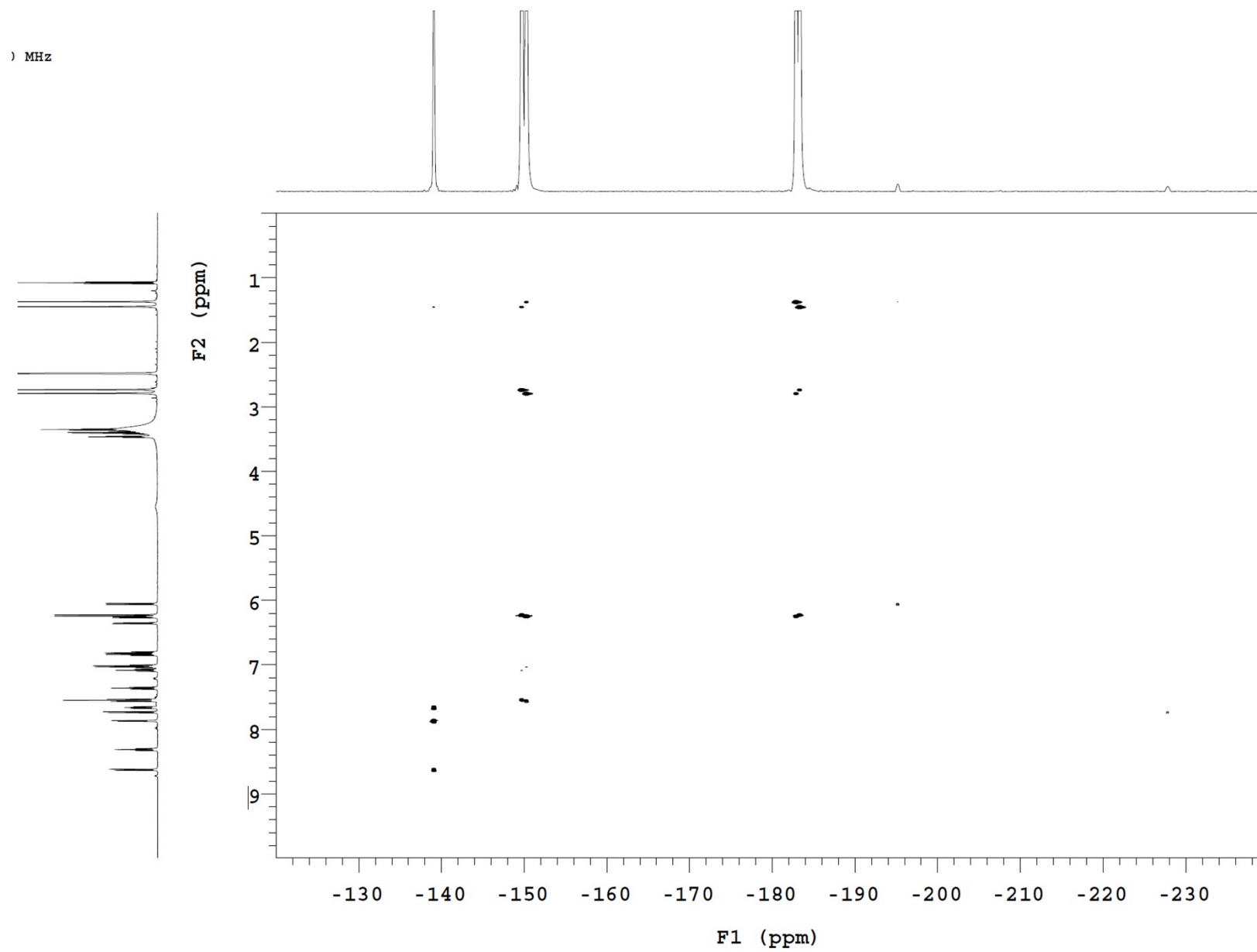
Fig. S12 ^{1}H, ^{13}C and ^{1}H-^{15}N HMBC NMR spectrum of **4** in DMSO-d_6 solution

a)

b)
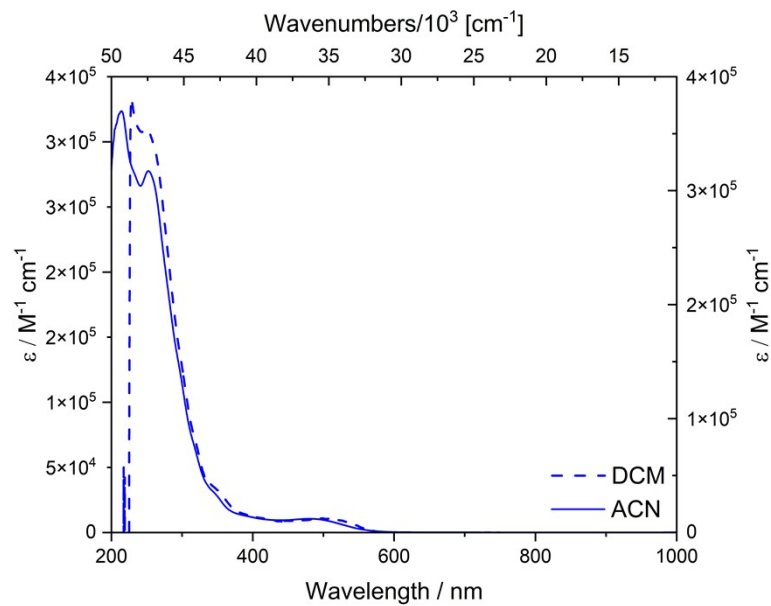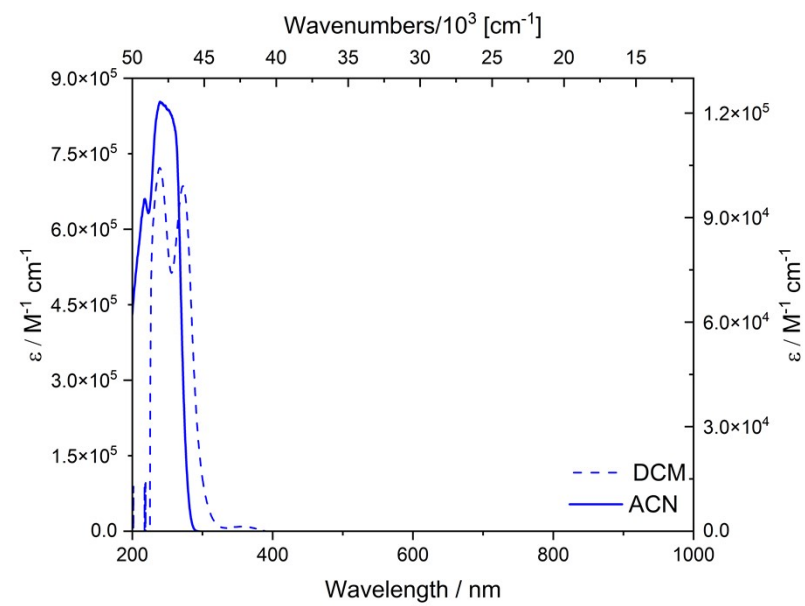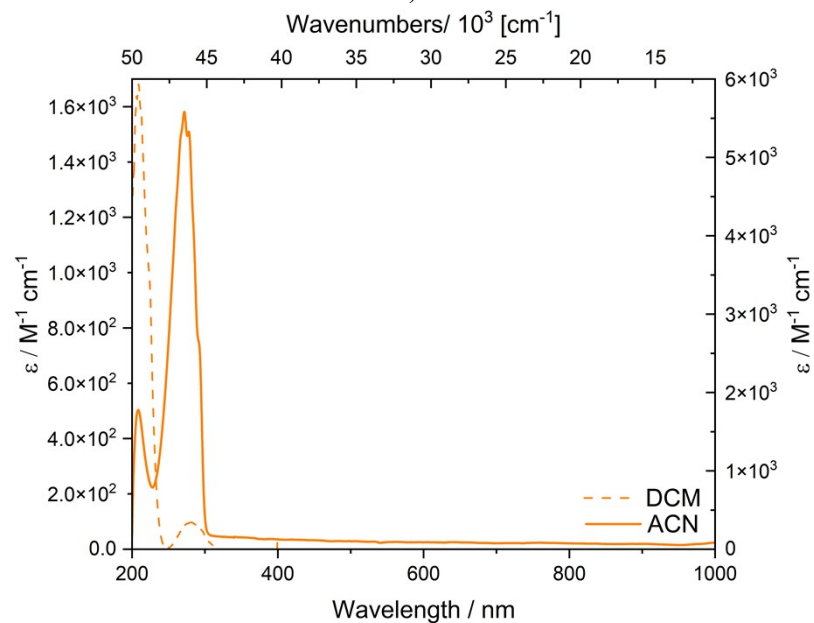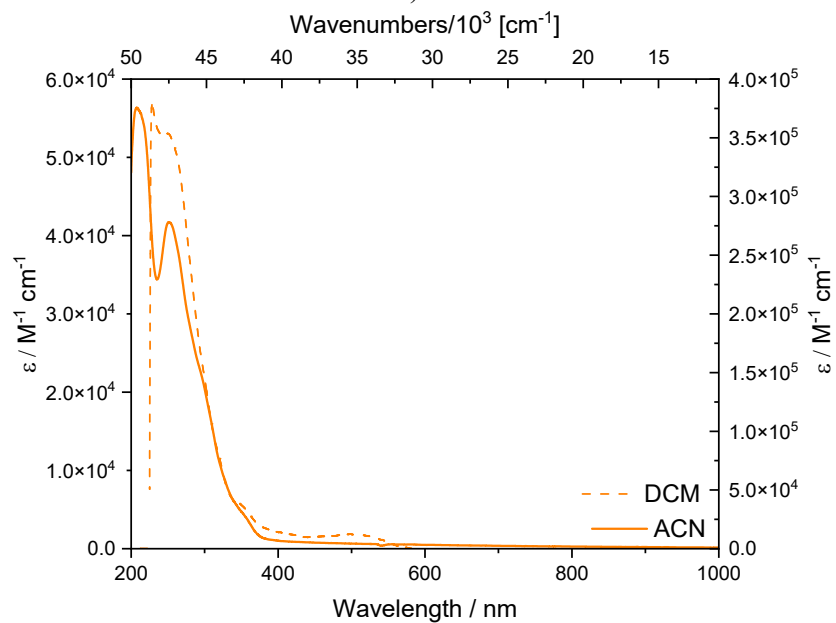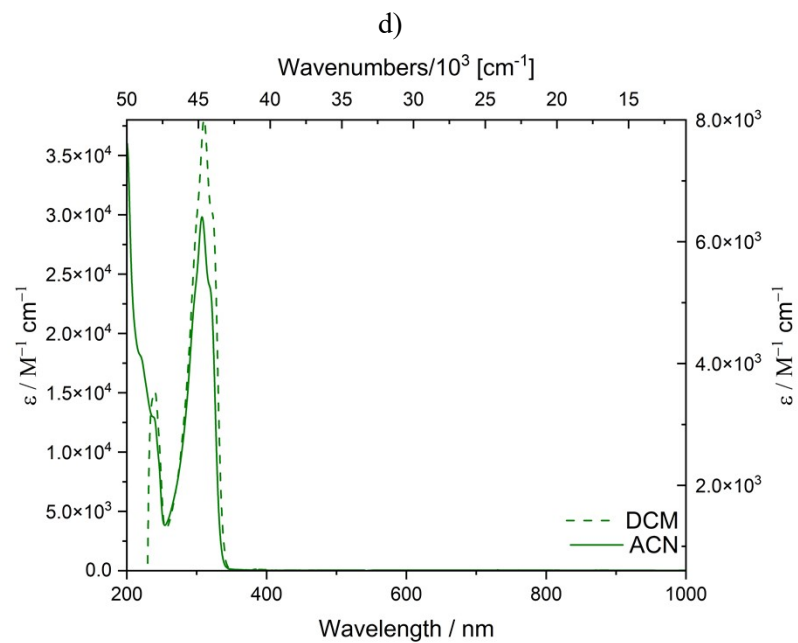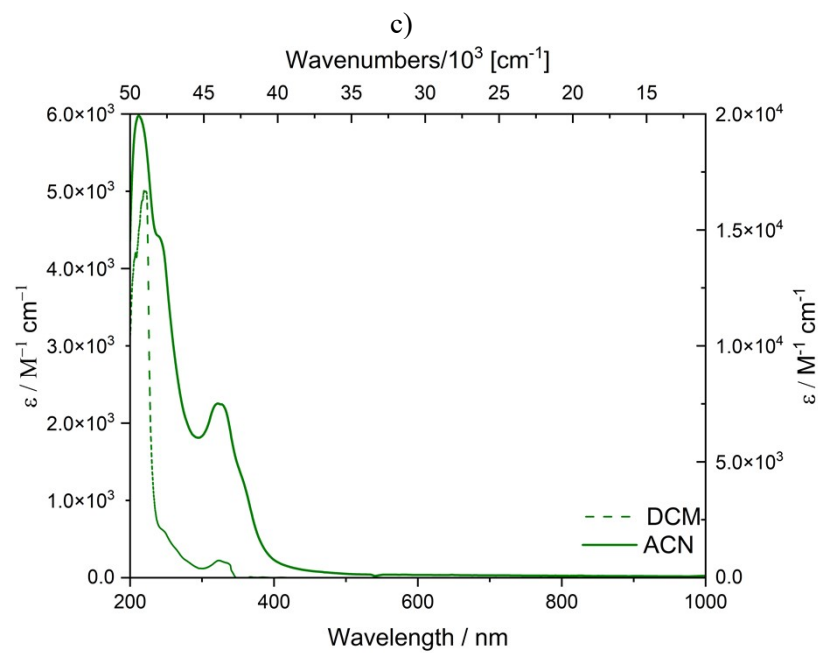
Fig. S13 Absorption spectra of complexes: (a) **2**, (c) **3**, (e) **4** and free ligands: (b) Py$_2$CO, (d) H$_2$biim, (f) PyBIm in DCM (CH$_2$Cl$_2$) (---) and ACN (CH$_3$CN) (—) solution at room temperature.
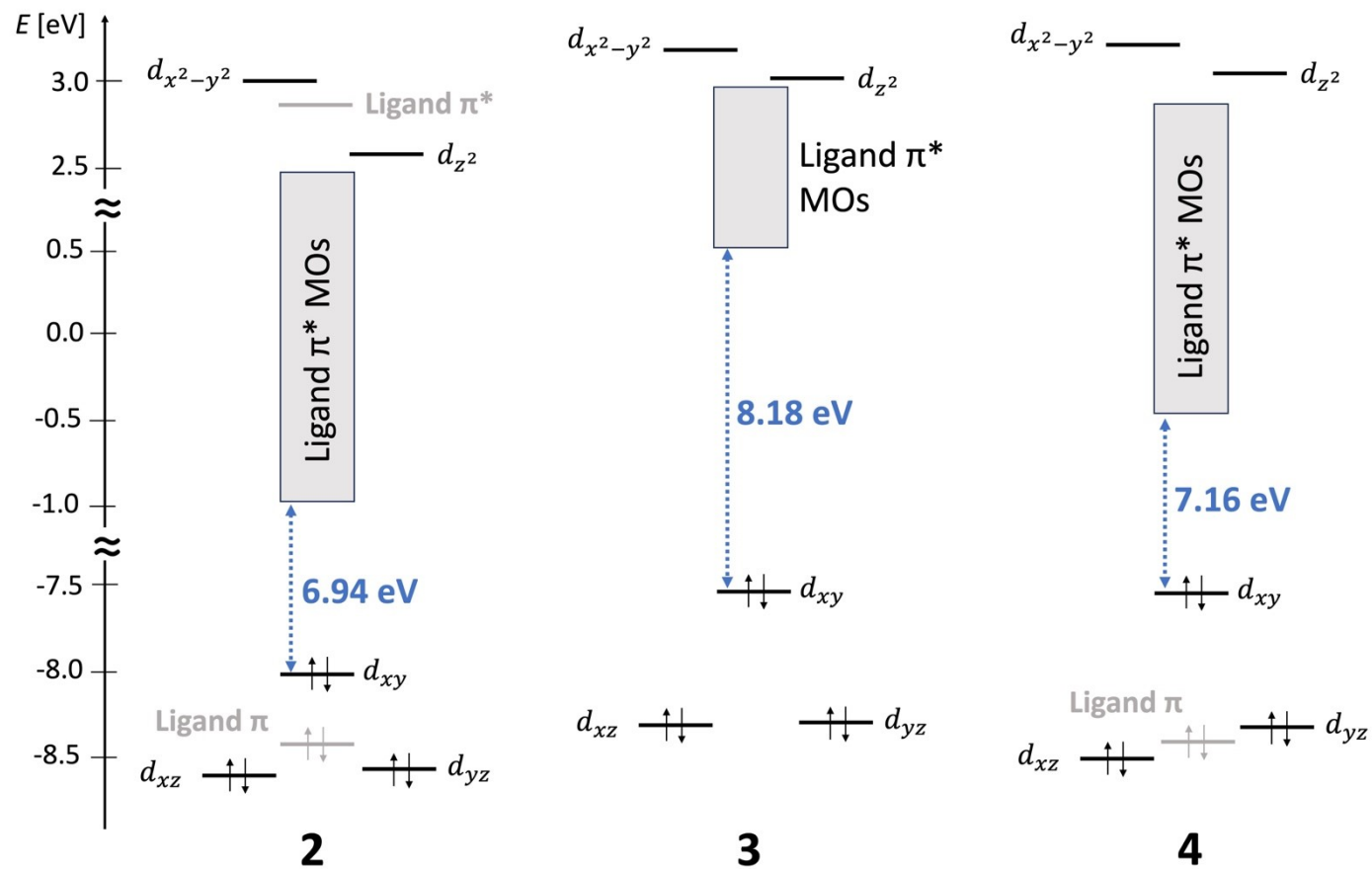
Fig. S14 Diagram of frontiers molecular orbitals of complexes **2-4**. Ir-centered and ligand-centered canonical orbitals are shown in black and gray, respectively. The HOMO-LUMO gap is highlighted in blue. Please note breaks in energy scale.
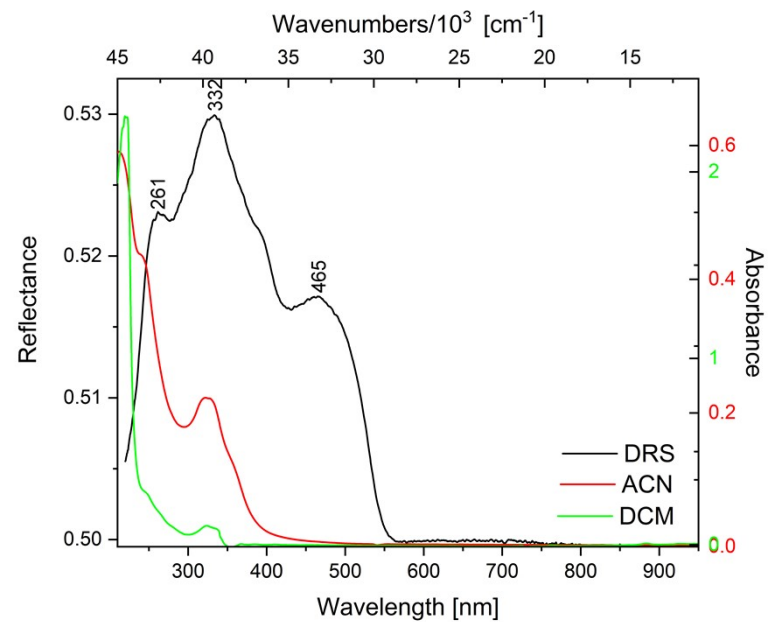
Fig. S15 Spectra of complex **4** in ACN and DCM solution and in solid state (DRS).
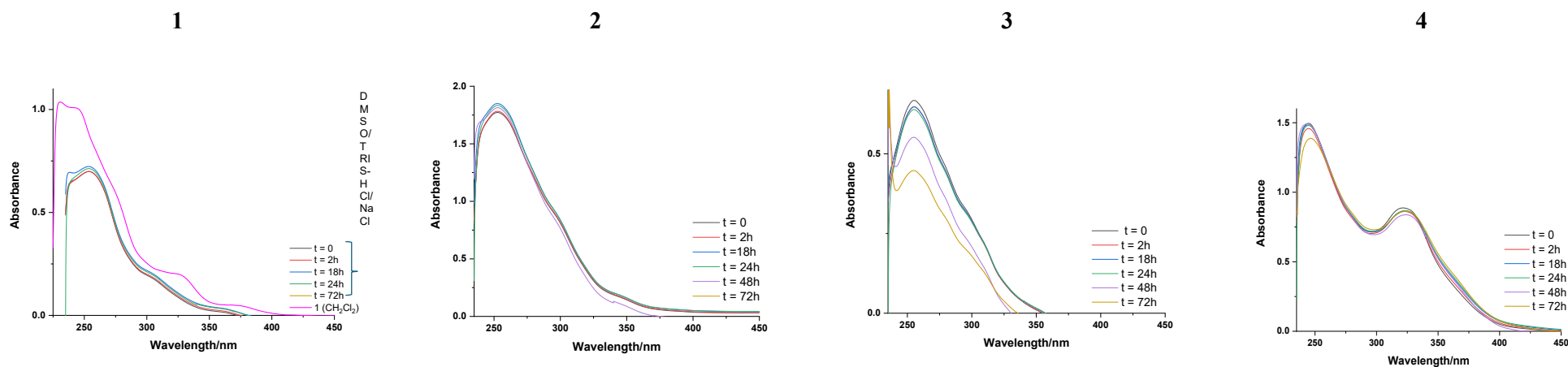
Fig. S16 UV-Vis absorption spectra of iridium complexes in DMSO/TRIS-HCl/NaCl solution over a period of 72 h (in spectrum of complex **1** comparison with CH_2Cl_2 solution spectrum).

34

0 h

24 h

48 h

a) 35
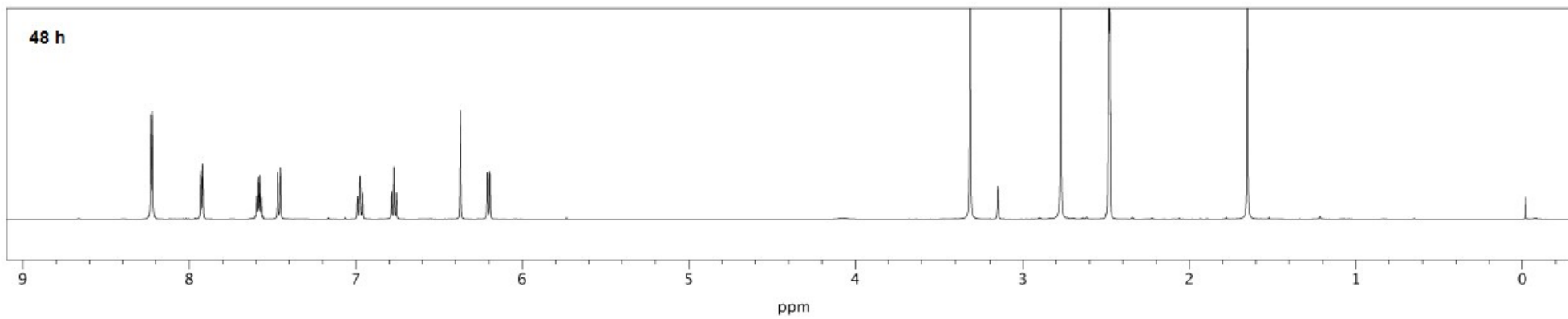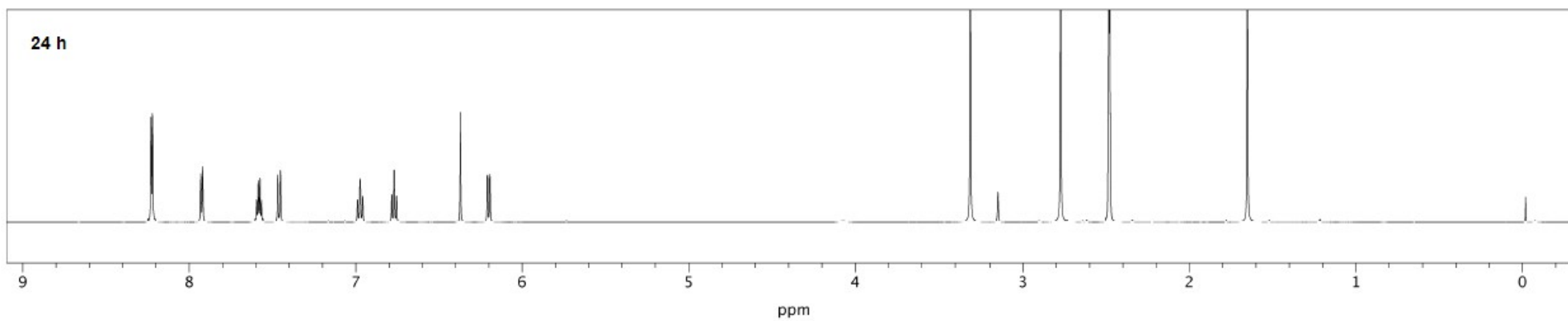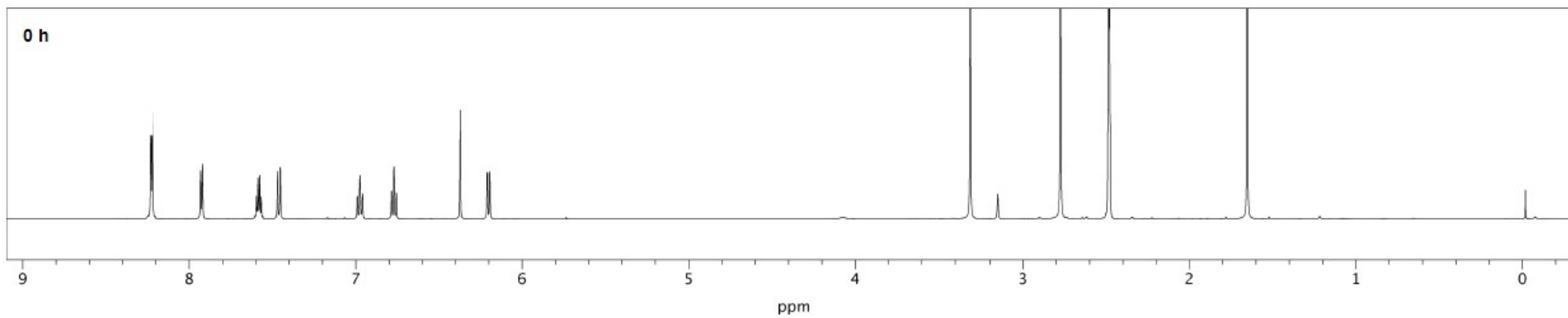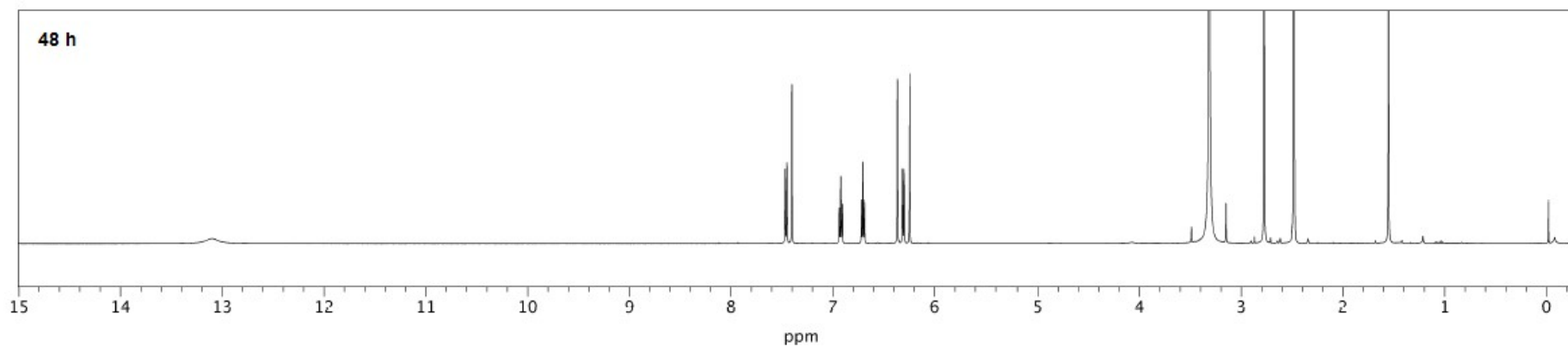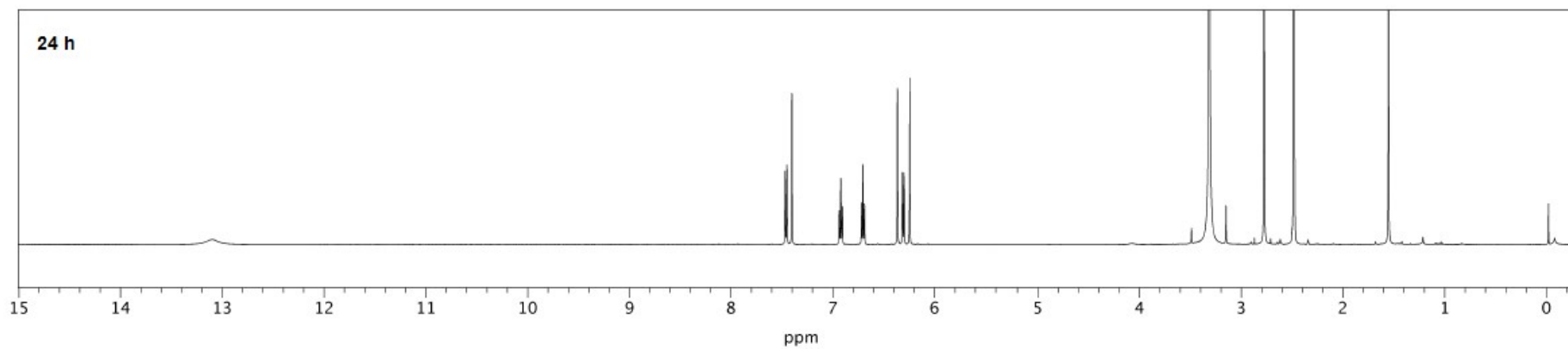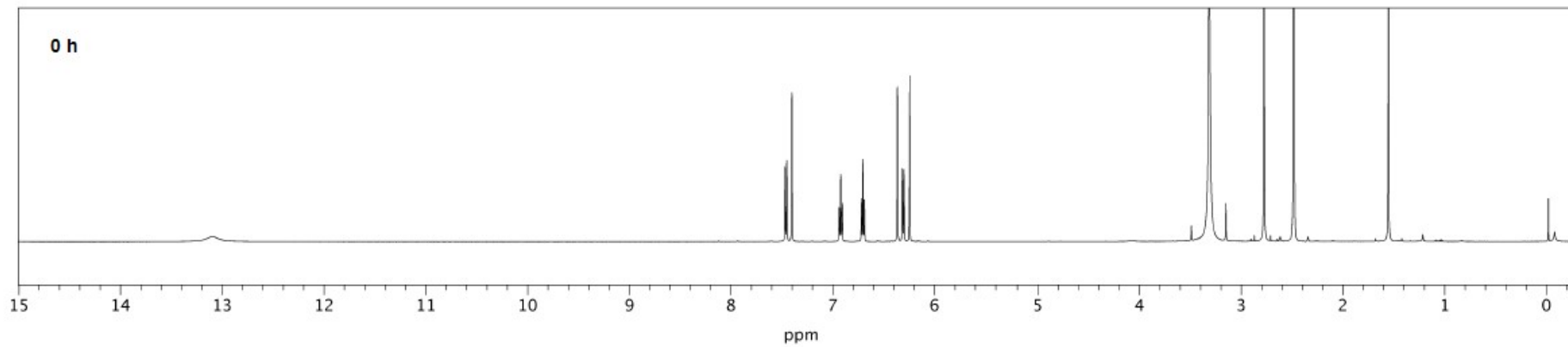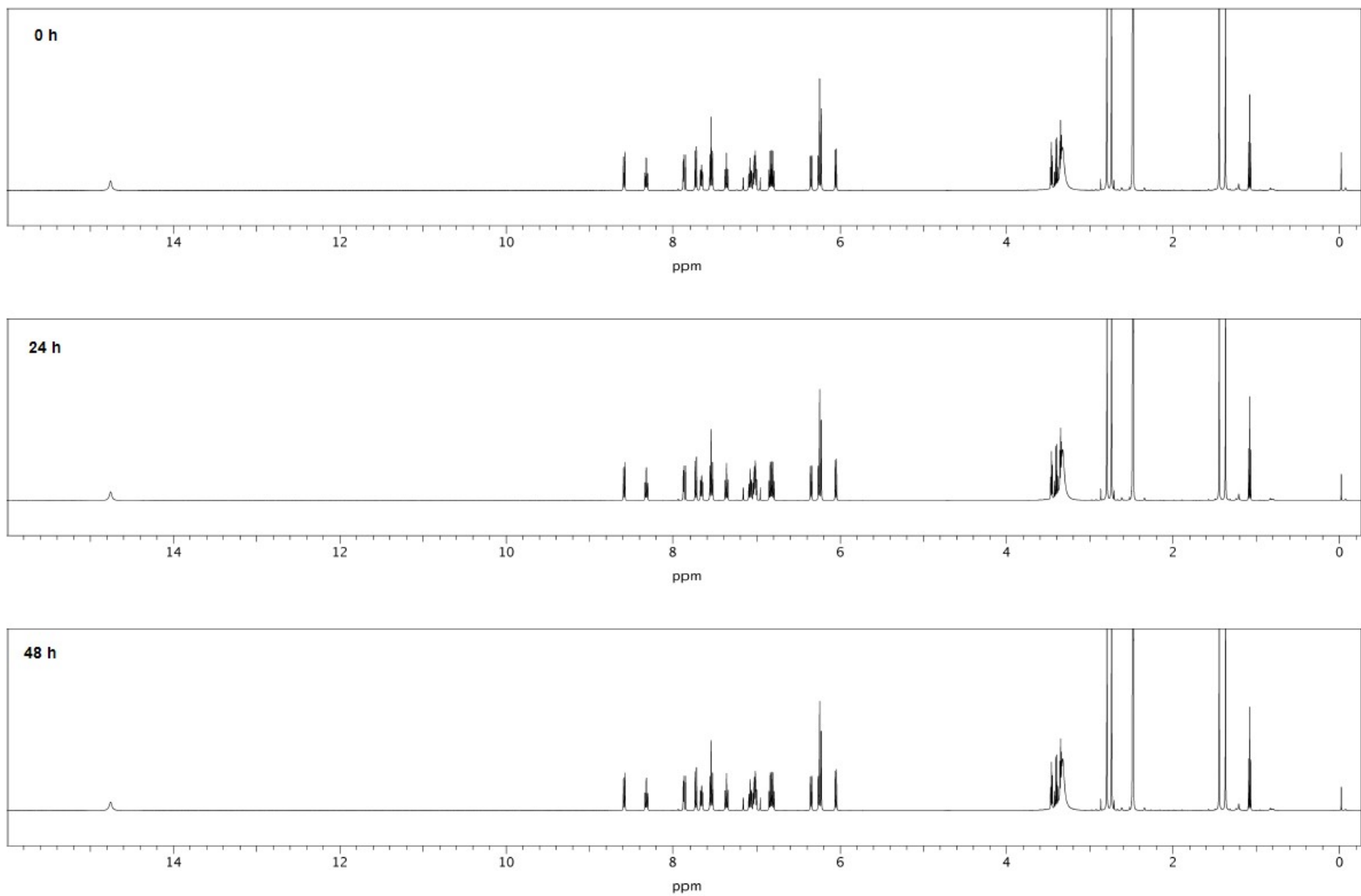
Fig. S17 ^{1}H NMR spectra of **2** (a), **3** (b) and **4** (c) over a period of 48 h.
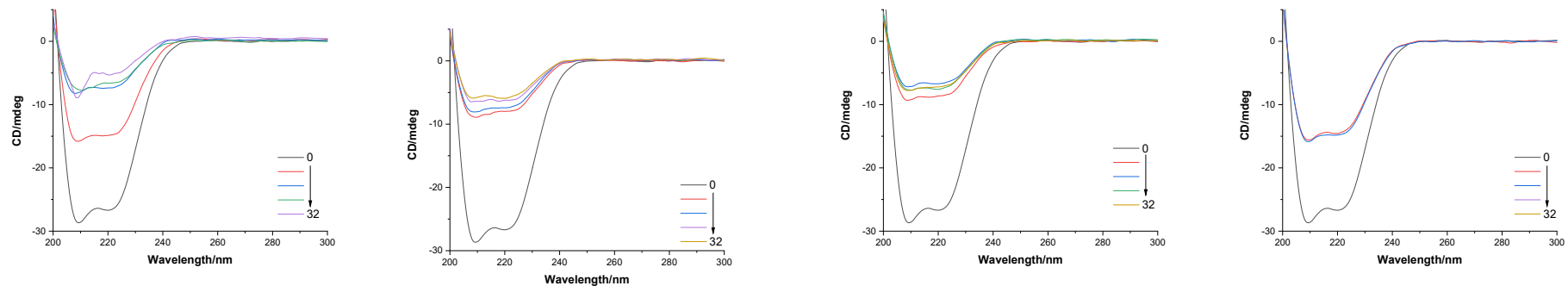
1

3

4
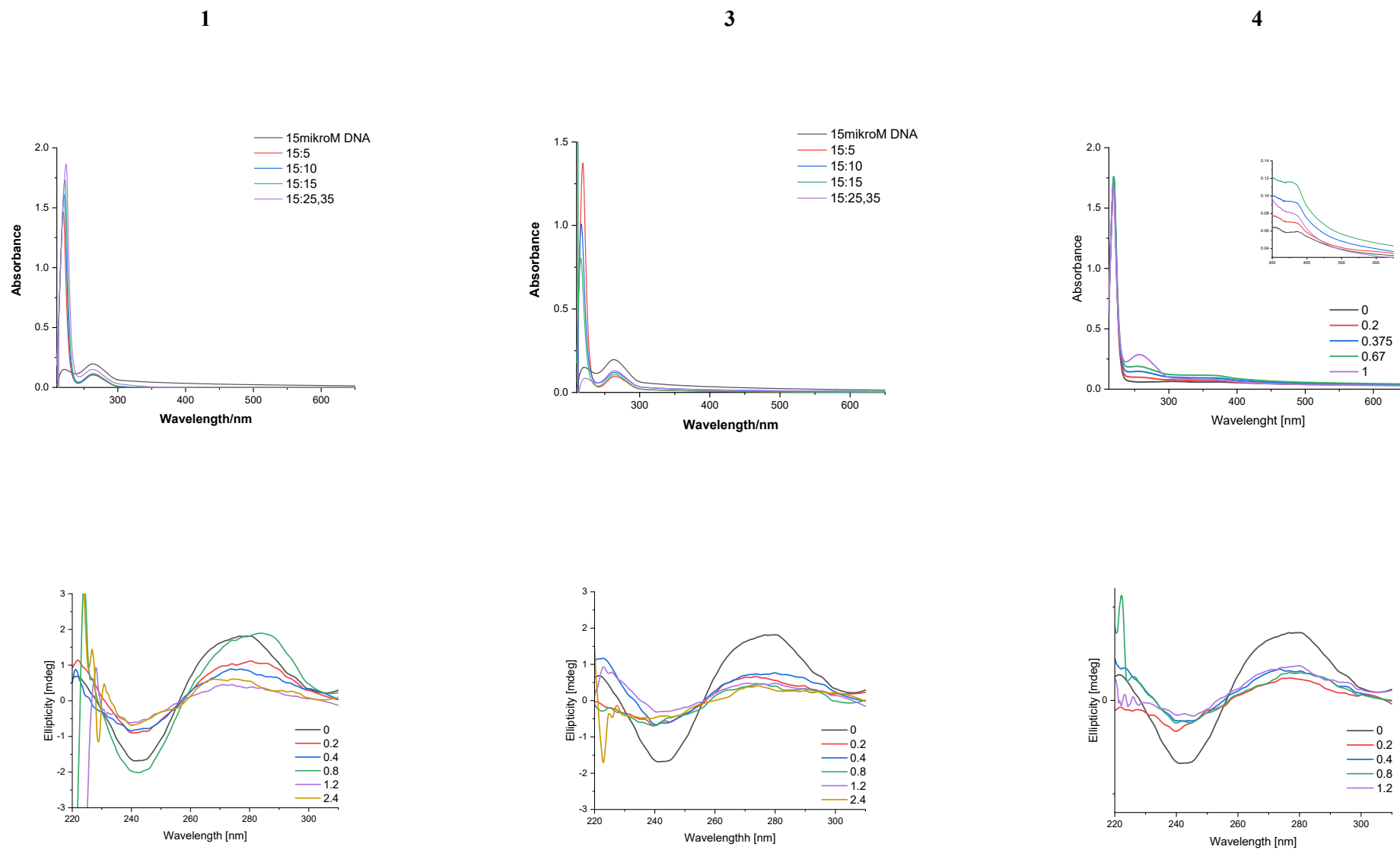
**Fig. S18** Absorption spectra (up) and CD spectra (down) of complexes **1**, **3** and **4** on addition of CT-DNA.
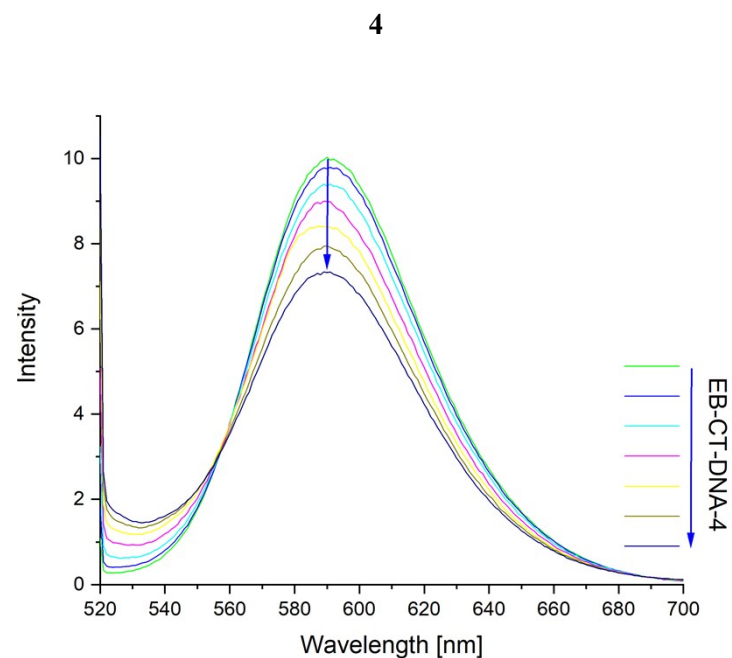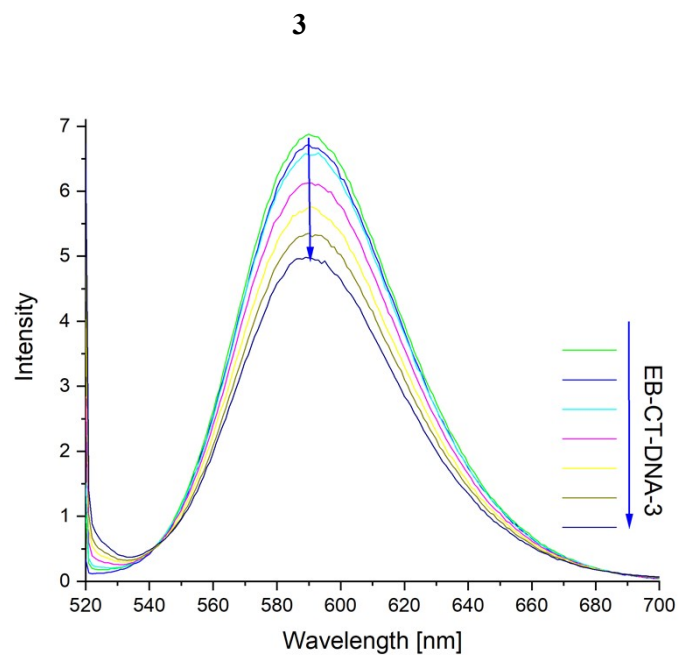
Fig. S19 Illustration of the fluorescence emission spectra (λ_{ex} 510 nm) when varying amounts of complex (a) **3** or (b) **4** are added to the stock solution of EB-CT-DNA. The arrow ($\downarrow$) indicates that the fluorescence intensity decreases with increasing amounts of complex.
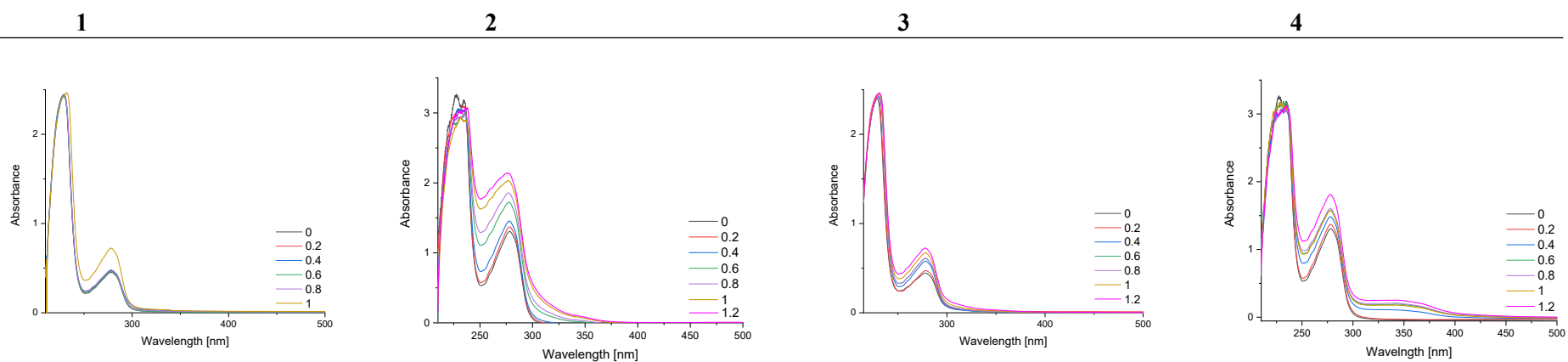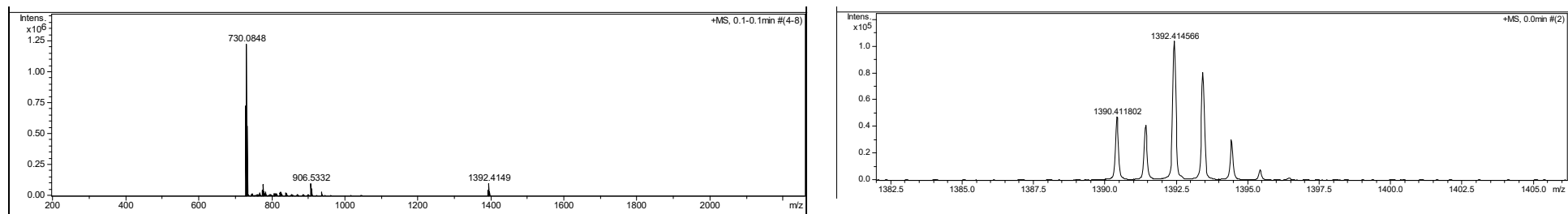
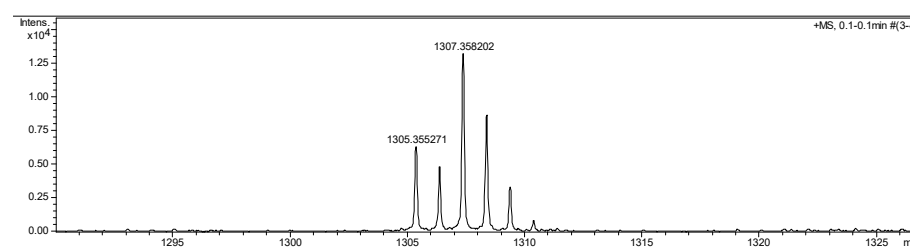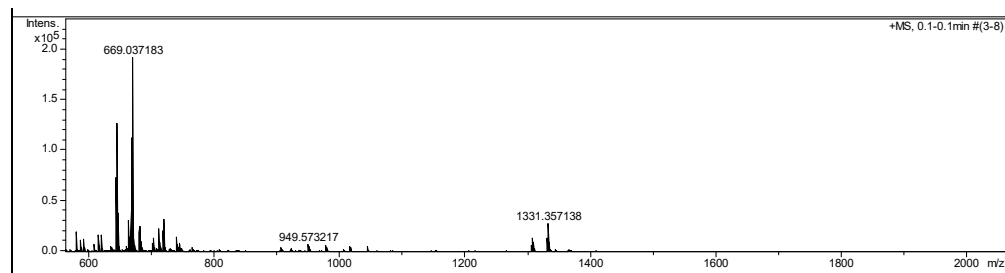**Fig. S20** Absorption spectra (up) and CD spectra (down) of complexes **1**-**4** on addition of BSA.
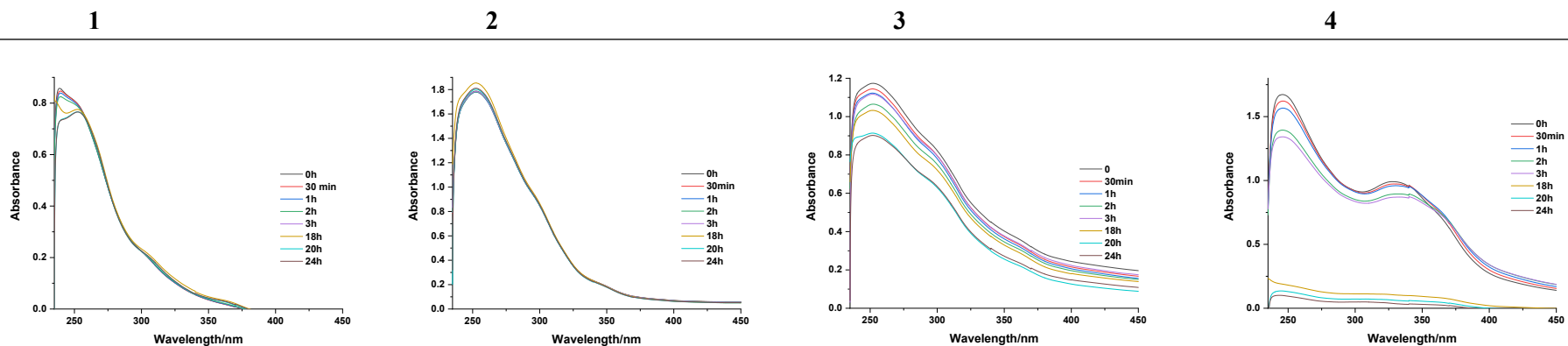
Fig. S21 UV-Vis spectra of complexes **1**-**4** in solution (95% H$_2$O /5% DMSO) in the presence of 20 mM GSH recorded over 24 hours.
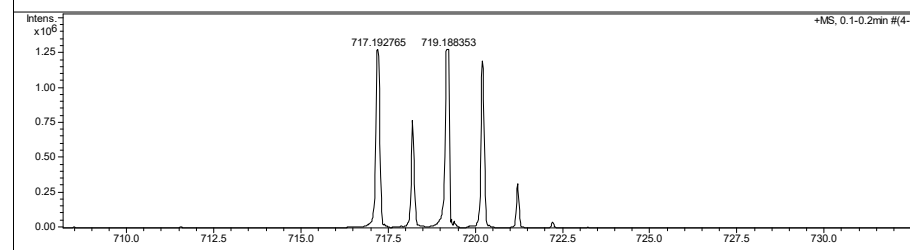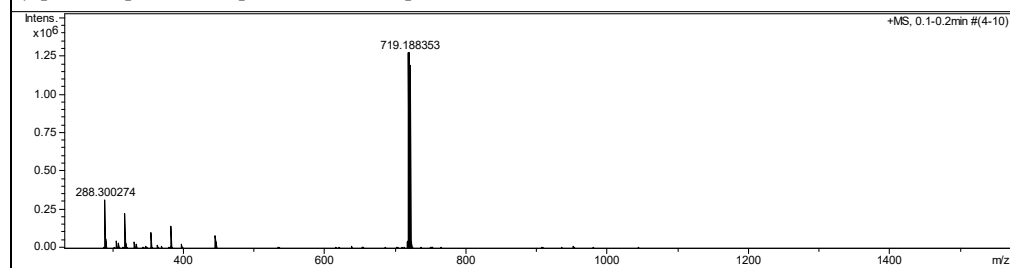
a) $[M-PF_6^-]^+$ 730.22, $[M+GSSG+NHCH_3+NH_4]^+$ 1390.4531072
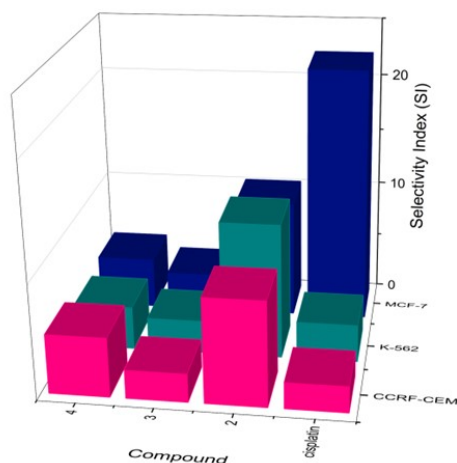

b) $[M-PF_6^-]^+$ 669.20, $[M+GSSG^-+Na]^+$ 1305.3561726

c) $[M-PF6]^+$ 719.20



d) $[M-H]^-$ 306.0759776, $[2M-H]^-$ 613.1597798, $[3M-H]^-$ 920.243582

Fig. S22 ESI-MS of GSH mixed with complexes (a) **4**, (b) **3**, (c) **2** (positive mode) and (d) free GSH (0.5 mM) (negative mode).

41

Fig. S23 Comparison of selectivity indexes (SIs) values of the tested complexes and cisplatin. The SI was calculated for each compound according to the formula: $SI = (IC_{50}$ for the normal fibroblasts BJ)/(IC_{50} for the respective cancer cell line).
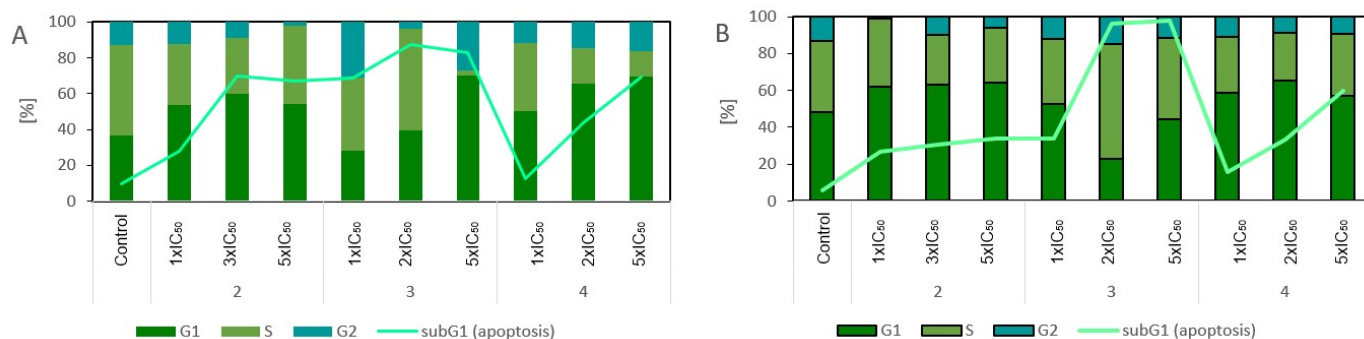
Fig. S24 Effects of compounds **2**, **3** and **4** on cell cycle (bars) and induction of apoptosis (line). The experiment corresponds to **Fig 8** in the main text which shows only effect on apoptosis. Panel A CCRF-CEM, panel B K-562.
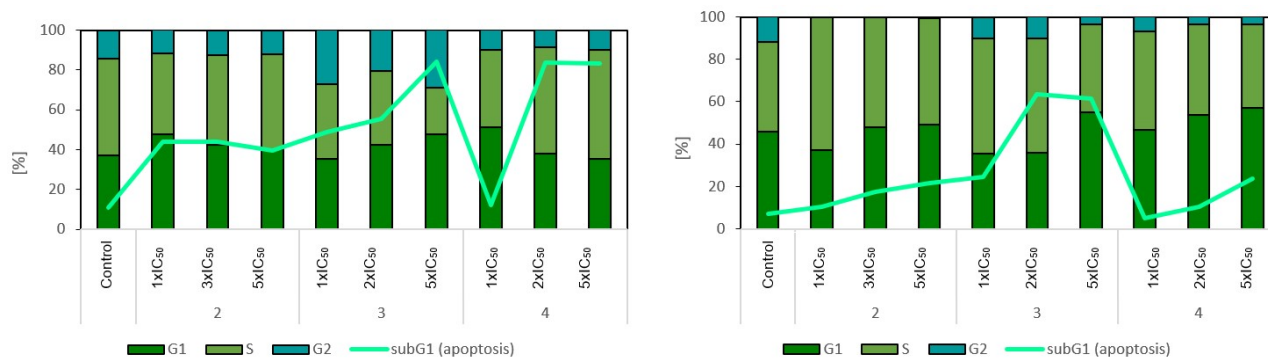
Fig. S25 Effects of compounds **2**, **3** and **4** on cell cycle (bars) and induction of apoptosis (line) on CCRF-CEM (left) and K-562 (right).
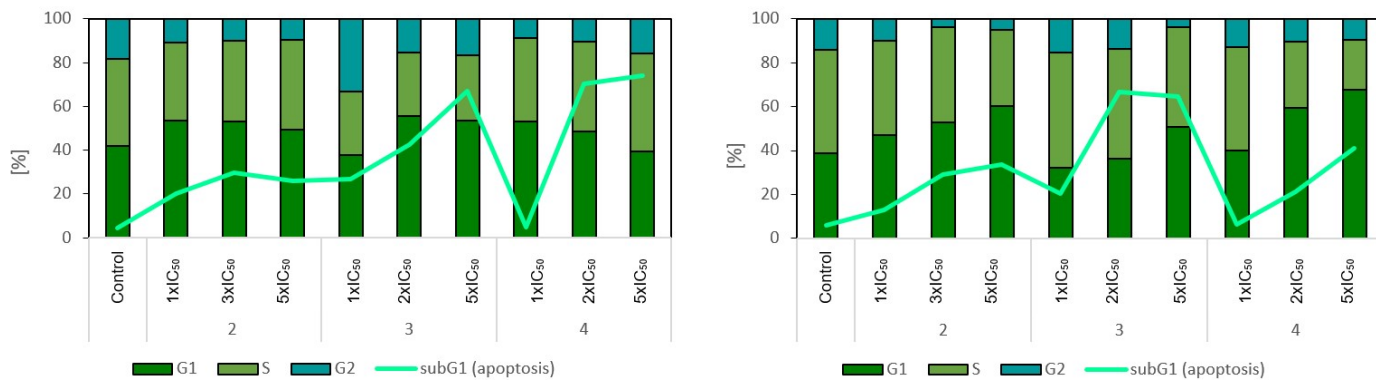
Fig. S26 Effects of compounds **2**, **3** and **4** on cell cycle (bars) and induction of apoptosis (line). In another 2 independent repetitions of the experiment on CCRF-CEM (up) and K-562 (down).

References

1   R. A. Velapoldi, *Proc. Conf. NBS, Gaithersburg, MD*, 1972, p. 231.
2   D. W. Marquardt, *J Soc Ind Appl Math*, 1963, **11**, 431–444.
3   J. Furrer, *Chem. Commun.*, 2010, **46**, 3396–3398.
4   E. Kupce and Freeman R., *Magn. Reson. Chem.*, 2007, **45**, 2–4.
5   D. S. Wishart, C. G. Bigam, J. Yao, F. Abildgaard, H. J. Dyson, E. Oldfield, J. L. Markley and B. D. Sykes, *J. Biomol. NMR*, 1995, **6**, 135–140.
6   F. Neese, *Wiley Interdiscip. Rev. Comput. Mol. Sci.*, 2022, **12**, 1–15.
7   J. Da Chai and M. Head-Gordon, *Phys. Chem. Chem. Phys.*, 2008, **10**, 6615–6620.
8   D. A. Pantazis, X. Y. Chen, C. R. Landis and F. Neese, *J. Chem. Theory Comput.*, 2008, **4**, 908–919.
9   V. Barone and M. Cossi, *J. Phys. Chem. A*, 1998, **102**, 1995–2001.
10   B. Helmich-Paris, B. de Souza, F. Neese and R. Izsák, *J. Chem. Phys.*, 2021, **155**, 104109.
11   STOE & Cie GmbH, X-Area 1.75, Software Package for Collecting Single-Crystal Data on STOE Area-Detector Diffractometers, for Image Processing, ScalingReflection Intensities and for Outlier Rejection, Darmstad, 2015.
12   G. M. Sheldrick, *Acta Crystallogr. Sect. A Found. Crystallogr.*, 2015, **71**, 3–8.
13   G. M. Sheldrick, *Acta Crystallogr. Sect. C Struct. Chem.*, 2015, **71**, 3–8.
14   O. V. Dolomanov, L. J. Bourhis, R. J. Gildea, J. A. K. Howard and H. Puschmann, *J. Appl. Crystallogr.*, 2009, **42**, 339–341.
15   S. P. Westrip, *J. Appl. Crystallogr.*, 2010, **43**, 920–925.
16   K. Brandenburg and B. G. Putz, H. Diamond-Crystal and Molecular Structure Visualisation Crystal Impac; 3.1 G; Rathausgasse 30, 1997.
17   A. L. Spek, *PLATON A Multipurpose Crystallographic Tool*, Utrecht Univeristy, The Netherlands, 2008.
18   A. Gilewska, B. Barszcz, J. Masternak, K. Kazimierczuk, J. Sitkowski, J. Wietrzyk and E. Turlej, *J. Biol. Inorg. Chem.*, 2019, **24**, 591–606.
19   Y. S. Ge, C. Jin, Z. Song, J. Q. Zhang, F. L. Jiang and Y. Liu, *Spectrochim. Acta - Part A Mol. Biomol. Spectrosc.*, 2014, **124**, 265–276.
20   Q. Wu, L. Y. Liu, S. Li, F. X. Wang, J. Li, Y. Qian, Z. Su, Z. W. Mao, P. J. Sadler and H. K. Liu, *J. Inorg. Biochem.*, 2018, **189**, 30–39.
21   A. B. P. Lever, *Inorganic Electronic Spectroscopy. Elsevier Publishing Co. Ltd., New York*, 1984.